İSTANBUL TECHNICAL UNIVERSITY ★ GRADUATE SCHOOL OF SCIENCE ENGINEERING AND TECHNOLOGY

GENERATION OF ZINC AND COPPER INCORPORATED OXIDE LAYERS ON TITANIUM BASED BIOMATERIALS

M.Sc. THESIS

Merve Kübra SAYGI

Department of Material Science and Engineering

Material Science and Engineering Programme

İSTANBUL TECHNICAL UNIVERSITY ★ GRADUATE SCHOOL OF SCIENCE ENGINEERING AND TECHNOLOGY

GENERATION OF ZINC AND COPPER INCORPORATED OXIDE LAYERS ON TITANIUM BASED BIOMATERIALS

M.Sc. THESIS

Merve Kübra SAYGI
(521131015)

Department of Material Science and Engineering

Material Science and Engineering Programme

Thesis Advisor: Prof. Dr. Hüseyin ÇİMENOĞLU

June 2016

İSTANBUL TEKNİK ÜNİVERSİTESİ ★ FEN BİLİMLERİ ENSTİTÜSÜ

TİTANYUM ESASLI BİYOLOJİK MALZEMELERDE ÇİNKO VE BAKIR KATKILANDIRILMIŞ OKSİT TABAKALARININ OLUŞTURULMASI

YÜKSEK LİSANS TEZİ

Merve Kübra SAYGI
(521131015)

Malzeme Bilimi ve Mühendisliği Anabilim Dalı

Malzeme Bilimi ve Mühendisliği Programı

Tez Danışmanı: Prof. Dr. Hüseyin ÇİMENOĞLU

Haziran 2016

Merve Kübra Saygı, a M.Sc. student of ITU Graduate School of Science and Technology student ID 521131015, successfully defended the thesis entitled "GENERATION OF ZINC AND COPPER INCORPORATED OXIDE LAYERS ON TITANIUM BASED BIOMATERIALS", which she prepared after fulfilling the requirements specified in the associated legislations, before the jury whose signatures are below.

Thesis Advisor :	**Prof. Dr. Hüseyin ÇİMENOĞLU** İstanbul Technical University	.....
Jury Members :	**Assoc. Prof. Dr. Murat BAYDOĞAN** Istanbul Technical University	.....
	Assoc. Prof. Dr. Erdem ATAR Gebze Technical University	.....

Date of Submission : 02 May 2016
Date of Defense : 06 June 2016

To my family and Emir,

FOREWORD

I would like to express my sincere gratitude to my supervisor Hüseyin ÇİMENOĞLU for his guidance and encouragement throughout my study. In addition to sharing with me his professional knowledge and experience.

I am thankful to Prof. Dr. Jennifer Patterson for giving me chance to work in Katholieke Universiteit Leuven. All my appreciation to MTM staffs for their priceless supports throughout my staying at KU Leuven and also I am greatly thankful to Prof. Dr. Jef Vleugels for his invaluable guiding.

Special thanks to my mentor Faiz MUHAFFEL, who led me and taught me a lot of things about my research. His help and novel ideas are very much appreciated.

In addition, I would like to give my honor to my friends Mine YÜCEL, Veronika SMISOVSKA, Adri GONZALEZ, Nesli TÜFEKÇİ, Büşra DANIŞ, Ksenia SOROKA, Petrica PETRAS, Mehmet Ali Recai ÖNAL, Sinem FİDAN, Dilek TEKER, Hilmi PAKSOY, Antonio Puppe DOS SANTOS for their generous help and technical support.

My deepest gratitude also goes to my family; my grandmothers Servet SAYGI & Ayşe BAŞARAN, my grandfathers İsmail SAYGI & Recep BAŞARAN and my mother Nurşen SAYGI, my father İsmail Hakkı SAYGI for their enormous emotional support.

Last but not least thanks to my friend, my love and my fiance; Emir AKTAN for his love, patience and support.

As Marie CURIE says “Be less curious about people and more curious about ideas.”

May 2016

Merve Kübra SAYGI
(Bioengineer)

TABLE OF CONTENTS

Page

ABBREVIATIONS

Cp	**:** Commercially pure
EDS	**:** Energy-dispersive X-Ray Spectroscopy
EPMA	**:** Electron Probe Micro Analyzer
HA	**:** Hydroxylapatite
ICP-OES	**:** Inductively Coupled Plasma Optical Emission Spectroscopy
MAO	**:** Micro Arc Oxidation
MQ	**:** Milli-Q
ppm	**:** parts per million
SBF	**:** Simulated Body Fluid
SEM	**:** Scanning Electron Microscope
SS	**:** Stainless Steel
OM	**:** Optical Microscope
XRD	**:** X-Ray Diffraction

SYMBOLS

Al	**:** Aluminium
Ca	**:** Calcium
Co	**:** Cobalt
Cr	**:** Chromium
Cu	**:** Copper
Fe	**:** Iron
O	**:** Oxygen
P	**:** Phosphorus
Ti	**:** Titanium
V	**:** Vanadium
Zn	**:** Zinc
σ	**:** Stress
ε	**:** Strain

LIST OF TABLES

Page

LIST OF FIGURES

Page

GENERATION OF ZINC AND COPPER INCORPORATED OXIDE LAYERS ON TITANIUM BASED BIOMATERIALS

SUMMARY

Metal implants are designed to remain in the body as a prothesis for solving bone damage problem. Bone tissue is damaged by the reason of osteoporosis, aging, accidents or similar reasons. The process of interaction between implant surface and bone tissue is obviously the key to the implant success. Surface morphology, composition, hydrophilicity and roughness are main factors of implant–bone tissue interaction and osseointegration. The aim of this study was to evaluate the bone-tissue response to a hydroxyapatite (HA) and calcium titanium oxide ($CaTiO_3$) containing biocompatible compound layer modified commerically pure titanium (composed of rutile and anatase) samples and Ti6Al4V samples by micro-arc oxidation method (MAO). During the oxidation process, an electrolyte is including calcium and phosphorus ions and samples act as anode material, also stainless steel container as catode material. In this study, CpTi-MAO, CpTi-MAO-Zn and CpTi-MAO-Cu have been developed on Grade 4 quality commercially pure titanium (CpTi), 64-MAO and 64-MAO-Zn have been developed on titanium alloy (Ti6Al4V) with a single step micro-arc oxidation process. Properties of surface, i.e. surface thickness, morphology/pore size, crystal structure, chemical composition, roughness and hydrophilicity, were characterized with various analytical techniques. Introduction of zinc acetate and copper acetate into the electrolyte of the MAO process led to incorporation of 4-5 wt.% Zn or 7 wt.% Cu into the multi-layer coating on the CpTi-based samples were measured by EPMA. 4.82wt.% Zn, 2.43 wt.% Cu was specified by EDS. The Zn-doped Ti6Al4V-based samples has been showed 5.38 wt.% Zn by EDS. Osteoconductive calcium phosphate coatings enhanced the bioactivity, zinc and copper incorporated oxide layers showed non-cytotoxic properties during the releasing test into simulated body fluids. According to the XRD examination of the CpTi-MAO, the coatings are primarily composed of anatase and rutile TiO_2 phases, α-titanium, hydroxylapatatite, $CaTiO_3$. Additionally, effect of zinc and copper into the multi-layer coating during micro-arc oxidation process may expose excellent antibacterial efficiency without decreasing the bioactivity.

.

TİTANYUM ESASLI BİYOLOJİK MALZEMELERDE ÇİNKO VE BAKIR KATKILANDIRILMIŞ OKSİT TABAKALARININ OLUŞTURULMASI

ÖZET

Canlı dokular, yaşlanma, kazalar, yaralanmalar ve başka bir çok sebepten ötürü kısmen zarar görebilir ya da tamamen kullanılamaz hale gelebilir. Canlı yapısında işlevsel aksaklıklar oluşturacak bu tür kayıpların telafi edilebilmesi için biyolojik açıdan uyumlu malzemeler geliştirilmektedir. Biyomalzeme olarak adlandırılan, vücudun işleyişine yardımcı olmak üzere tasarlanmış, vücut ile sürekli temas halde olabilecek, canlı dokuyla uyumlu malzemeler, temelde metalik biyomalzemeler, seramikler, polimerler ve kompozitler olarak sınıflandırılmaktadırlar. Yumuşak dokular için polimer bazlı malzemeler kullanılırken, kemik gibi sert dokularda metalik malzemeler tercih edilmektedir. Genellikle metalik biyomalzemeler, sert doku olarak tanımlanan kemik dokularında yaşanan kayıpları telafi etmek için kullanılırlar. Örneğin, titanyum alaşımları (örn. Ti6Al4V), kalça ve diz kemiklerinde oluşan kayıpları gidermek için geliştirilirken, diş implant uygulamalarında ise saf titanyum (Cp-Ti) kullanılmaktadır. Malzemelerin seçimi, kullanılacakları alanda beklenilen özelliklere göre belirlenir. Örneğin saf titanyum, düşük mekanik özelliklere sahip olmasından dolayı diş implant uygulamalarında tercih edilebilirken diz ve kalça protezleri gibi uzun süreli yük taşıyıcı olarak kullanılacak malzemelerde titanyum alaşımları tercih edilmelidir.

Titanyum ve alaşımları, canlı doku üzerinde toksik etki yaratmadığı için biyouyumlu malzeme olarak gösterilir. Ancak yüzeyinde bulunan oldukça inert titanyum oksit tabakası, implantın uygulanmasıyla birlikte beklenen yüzey etkileşimleri ve hücre tutunmasına olanak vermeyecek şekildedir. Karşılaşılan bu problemin çözümü olarak, biyouyumluluğu yüksek olan fakat biyoinert bir tabakaya sahip titanyum metalik malzemelerinin, bir takım yüzey işlemlerinden geçirilip, yüzeylerinin biyolojik olarak aktif bir hale getirilmesi düşünülebilir. Fakat biyoaktif bir yüzeyin elde edilmesi de malzemenin canlı dokuda kullanılmasına olanak sağlamaz. Kullanım bölgesine göre farklı türde bakterilere maruz kalacağı düşünülürse, biyomalzemelerin aynı zamanda da oluşabilecek bir biyofilm tehlikesine karşı içeriğinde antibakteriyel ajanları barındırmış olması beklenir.

Tüm bu problemlerin belirlenmesiyle birlikte, tez çalışmamda da biyolojik olarak uyumluluğuyla bilinen saf titanyum (CpTi) ve titanyum alaşımının (Ti6Al4V) yüzeylerini mikro ark oksidasyonu olarak adlandırılan yüzey kaplama yöntemiyle biyoaktif bir tabakayla kaplayarak, elde edilen seramik temelli biyoaktif tabakayı çeşitli karakterizasyon teknikleri ile inceleyip, antibakteriyel etki görebilme amacıyla da, yüzeyde ve iç katmanlarda metalik ajan birikimi sağlayabilmek için, yine aynı yöntem kullanarak, prosesin gerçekleştiği elektrolit sıvısı içerisine metal ajan kaynağı ekleyip ve böylece farklı yüzey morfolojisine sahip numuneler elde ettik. Böylece hem doku-implant etkileşimini arttırdığımızı hem de olası enfeksiyonları engellebileceğimiz hipotezini ortaya koyduk.

İlk olarak hidroksiapatit gibi dişlerin mine ve dentin tabasında ve kemikte bulunan biyoaktif kalsiyum tuzunun, mikro ark oksidasyonu ile titanyum temelli malzemelerin üzerine kaplayabilmeyi amaçladık. Mikro ark oksidasyon işlemi, metallerin yüzey modifikasyonu için kullanılan, elektrokimyasal esaslı bir yüzey modifikasyonu tekniğidir. Bu teknikte, genellikle bazik esaslı bir elektrolit çözeltisi içinde, anot (numune) ve katot (paslanmaz çelik bir konteyner kullanıldı) arasında yüksek bir voltaj uygulanır ve bu yüksek voltaj belirli bir kritik voltaj değerini aştığından malzeme üzerinde mikro ve nano boyutta kıvılcımlar oluşmaya başlar ve bir dizi karmaşık reaksiyon sonucunda numune yüzeyinde poroz bir oksit tabaka oluşur. Proses sırasında anot görevi görecek ve üzerinde kaplama oluşmasını istediğimiz numunemilerimizin bir grubu ticari saflıktaki titanyum iken diğeri titanyum alaşımı (Ti6Al4V) idi. Bu numuneler, uzun titanyum çubuklarından, 4 milimetre kalınlığında kesilmiş ve yüzeyde pürüzlülük gözle görülemeyecek seviyede azalana kadar zımpara işlemi yapılmıştır. Zımpara işlemi sonucunda hazır olan numuneler, 15'er dakika sırasıyla alkol, aseton ve son olarak saf su ile yıkanıp, kurulanarak temizlenmiştir. Ardından da mikro ark prosesi için elektrolit çözeltileri, istenilen kaplama doğrultusunda hazırlanmıştır. Bir numaralı elektrolit çözeltisi, kalsiyum ve fosfor kaynağı olacak kimyasallar ile hazırlanırken, iki numaralı elektolit çözeltisi, kalsiyum ve fosfor kaynaklarının dışında çinko kaynağı da içermektedir. Üç numaralı elektrolit çözeltisi ise proses sonunda kalsiyum, fosfor ve bakır birikimini sağlayacak kimyasallarla oluşturulmuştur.

Tüm bu bilgiler ışığında, titanyum malzemelerin, seramik bir kaplama ile belirli bir kalınlıkta kaplanması amacıyla hazırladığımız oksidasyon işlemi için gerekli elektrolit çözeltisine daldırılmasının ardından, daha önceden optimize edilmiş oksidasyon parametreleriyle (voltaj, zaman parametreleri gibi) titanyum malzemenin üzerinde kalsiyum ve fosforca zengin poroz ve oksit bir tabaka oluşturulmuştur. Anodun saf titanyum olduğu proses sonucunda oluşmuş numuneler, CpTi-MAO olarak kodlanmış, anodun titanyum alaşımı olduğu proses sonucunda seramik kaplama ile kaplanmış numuneler ise 64-MAO (bazı yerlerde Ti6Al4V+MAO olarak da geçmektedir.) olarak kodlanmıştır.

Kalsiyum ve fosforca zengin oksit ve porozlu yapının yeterli olmaması durumdan ötürü, bir diğer işlemle metalik ajan içermesi amaçlanan yeni numuneler hazırlanmıştır. Elektrolit çözeltisine kalsiyum, fosfat tuzlarının yanında, çinko asetat da eklenmiştir, CpTi-MAO ve 64-MAO numunelerinin hazırlandığı aynı mikro ark oksidasyon parametreleri ile anodun CpTi olduğu prosesin sonucunda, CpTi-MAO-Zn olarak kodlanan numuneler hazırlanmış, anodun Ti6Al4V olduğu prosesin sonucunda da 64-MAO-Zn numuneleri hazırlanmıştır. Aynı zamanda, metalik ajan olarak çinko dışında bir başka antibakteriyel özellik gösteren ajanın kullanılması düşünülmüş, birkaç adet bakır ajan içeren numuneler de hazırlanmıştır. Bunlar da CpTi-MAO-Cu olarak kodlanmış, diğer hazırlanmış numunelerle birlikte yüzey analizlerine tabii tutulmuşlardır.

Antibakteriyel ajanın seçimi konusunda literatür araştırılmasına gidilmiş, literatürde sıklıkla görülen gümüş ajan katkılanması çalışmaları incelenmiş, uzun vadede canlı dokuda toksik etki yaratmasıyla bilinen gümüşün yerine canlı dokuda toksik etki yarattığıyla ilgili kanıtlanmış bir sonucun bulunmadığı, literatürde de oldukça yeni olan çinko ajan üzerinden gidilmesine karar verilmiştir. Çinkonun yapı üzerindeki etkisinin daha rahat kıyaslanabilir olması ve aynı zamanda da alternatif yaratabilmek amaçlı yukarıda da belirtildiği gibi bakır ajan içerikli numuneler de hazıralanmıştır.

Numunelerin hazırlık işlemlerinin tamamlanmasıyla birlikte, saf su ile yıkanmış ve oda sıcaklığında kurumaya bırakılmışlardır. Kuruma işleminin ardından da mikroskobik incelemeler, X-ışınları analizi, pürüzlülük ölçümleri, temas açısı ölçümleri yapılmıştır. Metalik ajanların, yapay vücut sıvısı (SBF) ve saf su içerisindeki salınım davranışları da incelenmiştir. Mikroskobik incelemeler, EDS donanımlı taramalı elektron mikroskobu (SEM) ile gerçekleştirilmiştir. Kesit numuneleri hazırlanarak, numunelerin kimyasal kompozisyonlarının haritalandırma yöntemi ile belirlenebilmesi için de elektron-probe mikro analizi (EPMA) olarak bilinen yöntem kullanılmıştır. Oksit tabakasının kalitatif faz analizi için CuKα radyasyonu kullanan bir X-ışını difraktometresi (XRD, GBC-MMA) ile gerçekleştirilmiştir. Numune yüzeylerinde oluşan kaplamaya ait yüzey pürüzlülüğü profilometre ile incelenemiştir. Yapay vücut sıvısında ve saf suda bekletilen numunelerin yüzey salınımlarına endüktif kuplajlı plazma optik emisyon spektral analizi (ICP-OES) yöntemi ile bakılmıştır. Islatma açısı ölçümü yapmak amacı ile KSV CAM200 cihazında malzeme yüzeyine 5µl saf su damlatılıp ölçüm yapılarak ortalama yüzey ıslanma miktarları açısal olarak belirtilmiştir.

Deneysel çalışmalar sonucunda elde edilen bulgular ışığında yapı-özellik ilişkisi kurulacak ve optimum özelliklerin elde edildiği MAO yöntemi ile elde edilen porozlu yüzeye antibakteriyel test uygulaması yapılacaktır.

1. INTRODUCTION

Bone tissue is frequently injured due to osteoporosis, aging, accidents or similar other reasons. Metal implants are designed to remain in the body as a prothesis that can solve bone damage problem. The process of interaction between implant surface and bone tissue is obviously the key to the implant success. Surface morphology, composition, hydrophilicity and roughness are main factors of implant–bone tissue interaction and osseointegration.

Stainless steel, cobalt chromium, titanium and titanium alloys (i.e., Ti-6Al-4V) are the materials which are commonly used in in metal implants for bone regeneration [1-3]. Many different type of metals are used in implantology, but during recent years there has been a clear trend the direction of titanium because of its excellent properties: low elastic modulus (close to bone), low density, light weight, non-magnetic properties, high biocompatibility and corrosion resistance. Unalloyed titanium is usually used for dental implant such as imitation teeth [4-6]. But unalloyed titanium in the other words commercially pure titanium can be identified as bioinert because of its protective oxide layer when exposed to air or water. The bulk of dental implants is composed of solid titanium, while surface treatments create porous surfaces by way of their bioinert property [7,8]. Surfaces can be changed by acid etching, by blasting with several substances, by coatings, or by combinations of such treatments.

Various techniques (e.g., electrochemical oxidation) have been used to produce the porous surface and promote bioactivity and cell attachment [9-11]. Recently, micro arc oxidation (MAO) (an environment-friendly technology) is commonly used to create coatings with special properties such as bioactivity. This process produces preferential deposition of a hydroxyapatite and calcium titanium oxide ($CaTiO_3$) containing biocompatible compound layer on the titanium oxide layer (composed of rutile and anatase).

Besides, bacterial infection can lead to a higher risk of implant failure, after implantation of dental implant is still one of the biggest complications. Clinical studies have shown that 7.7% implant failure over a 5 year-period [12].

Bacteriside capability of Zn has been known for several years [13]. Zn-doped Ti-based have on antibacterial effect on *Staphylococcus aureus* and *Escherichia coli* by leading to cell membrane degradation and cytoplasma dropping [14]. Zinc oxide (ZnO) also has significiant antibacterial effects on different species of microorganisms [15].

Past publications have shown that treating a titanium surface by MAO provides a perfect surface for bone – implant interaction [16,17]. And also one of the biggest complication is bacterial infection problem can be solved with metallic agents for a long stage.

The aim of this study was to exhibit that HA and $CaTiO_3$ containing biocompatible compound layer on the TiO_2 layer with Zinc agents will show excellent properties for each stage of healing.

2. BIOMATERIALS

Living tissues can be damaged by diseases, aging, trauma, accidents, etc. Biological materials in the other words biomaterials are synthetic or natural materials that are used to directly replace, amend or make improvement the damaged tissues. This biomaterials can be used individual or in combination with different materials which are used in living tissues at variant times. Several works have been done on providing excellent properties and efficiencies of biomaterials.

The invention of first generation biomaterials in the between the 60s and the 70s, synthetic materials started to be a subject of interest for using inside of the human body. However, the first biomaterials date back to ancient civilization. Synthetic ears, teeth, eyes and noses have been found on Egyptian mummies. Asian civilization such as Chinese and Indians used binders, waxes, and tissues in restructuring damaged or missing units of the body. In previous years, progression in biomaterials, surgical methods and sterilization techniques have allowed the use of these synthetic materials in lots of new ways. Nowadays, many devices and implants are utilized by medical practice. Synthetic materials in the other words in form of biomaterials (orthopedic and dental implants, sutures, spinal screws, joint replacements, vascular grafts, lenses and etc.) and medical instruments (biosensors, blood tubes, artificial hearts and etc.) are commonly used to replace and/or enhance function of traumatized or regeneration of tissues or organs, to conduce in healing, to advance function, to fix abnormalities and thereby improve the quality of life of the patients [18].

Previously all type of natural materials such as cements, woods, rubbers or tissues from organic materials and processed materials such as metals or glasses were used as biological materials predicate on trial. The responses of host tissue to these kind of materials were intensely different. Over the last 30 years significant improvement has been made in methods that shows the intereactions between lifeless materials and living tissues [19].

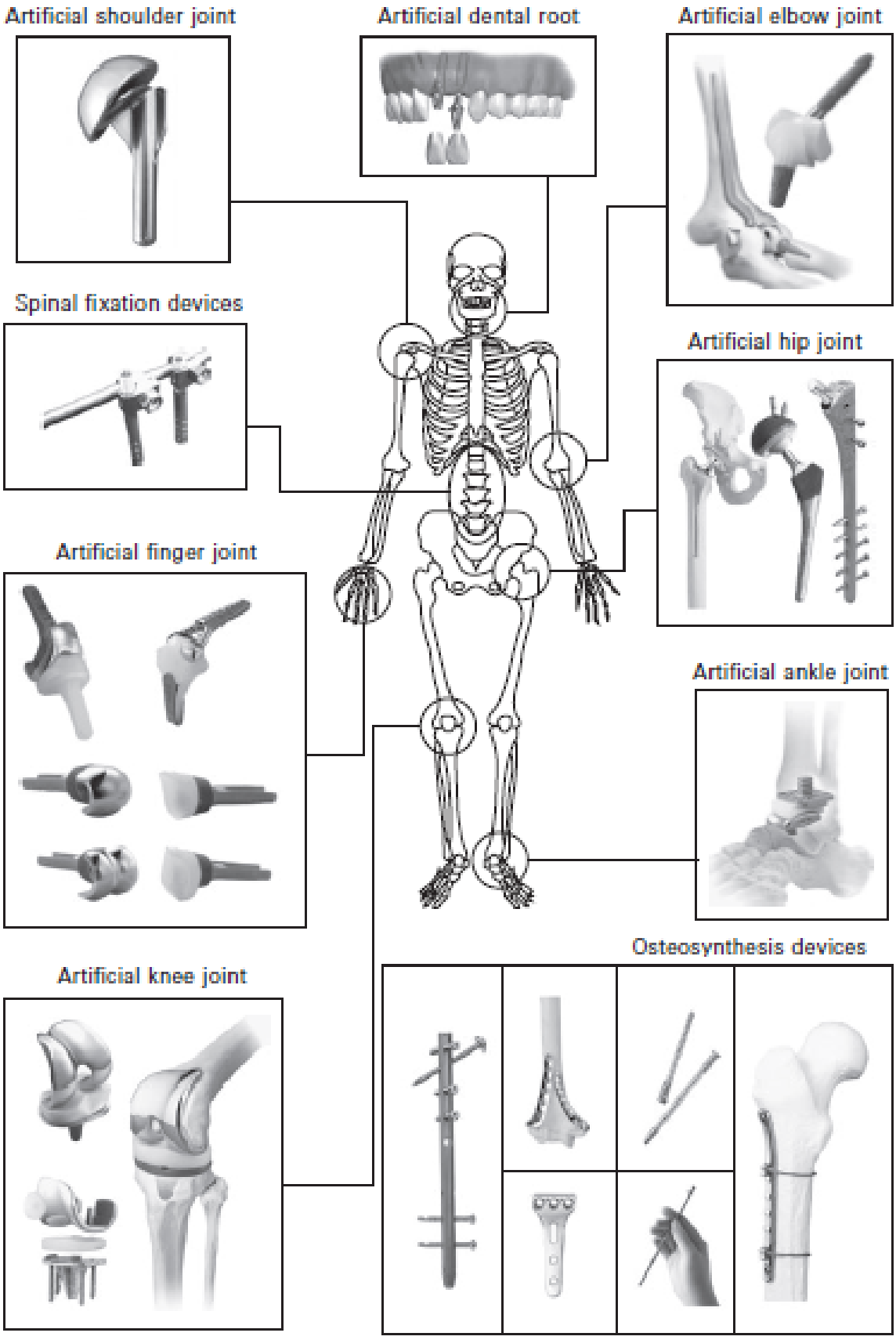

Figure 2.1 : The most commonly used biomaterials [18].

Scientists have lexicalised the words “biomaterial” and “biocompatibility” to specify the biological property of materials. Materials which can be described as biomaterials, the biocompatibility refers to the ability of a material with an appropriate host response in a specific situation [20]. The fundamental objective of using biomaterials is to develop human health and life by restoring or enhancing the function of living tissues and organs in the human body. It is crucial to understand relationships between the properties, functions and structures of biological materials. Hereby, three directions of study on the sucject of biomaterials can be visualized: biological materials, implant materials, and interaction between the two in the body.

The success of a biological material in, other words implant material, is extremely dependent on three major factors: the properties of implant, biocompatibility of the implant material, the health circumstance of the patient, the proficiency of the surgeon who implants and controls its operation, operation place and devices conditions. Requirements for an implants are:

- Acceptance of the implant to the host surface, i.e., biocompatibility (this is a main term and includes points 2 and 3)
- Nonallergenic
- Nonimmunogenic
- Nontoxic
- Noncarcinogenic
- Chemically inert and stable (any degredation depends on time)
- Not corrode or degrade in vivo
- Sufficient mechanical strength
- Sufficient fatigue life
- Wellness engineering design
- Convenient density and weight
- Easy to be machinability and allow for processing large-scale production, inexpensive, reproducible [21].

Table 2.1 : Classes of biomaterials [21].

Materials	Advantages	Disadvantages	Examples
Ceramics (alumina, zirconia, hydroxylapatite)	Highly biocompatible	Brittle, non-elastic. low tension strength	Dental and orthopeadic implants
Metals (titanium and alloys, stainless steels, etc.)	Strong, tough, ductile	Low corrosion resistivity, hard to be produced, heavy	Bone plates and screws, dental implants, joint replacements
Polymers (nylon, silicone, polyester, etc.)	Elastic, easy to produce	Weak, time dependent deformation, can be degradable	Ear, nose, sutures
Composites (carbon-carbon, fiber reinforced bone cement)	Strong, tailor-made	Expensive, hard to make	Bone cement, dental resin

Table 2.1 shows some of the advantages, disadvantages, and applications of four groups of unnatural materials used as an implant material.

2.1 Classification of Biomaterials

The four main classes of biomaterials are defined as (1) metallic materials, (2) polymers, (3) ceramics, (4) composites.

2.1.1 Metallic materials

Metallic materials are widely used for load bearing implants, external and internal fixation devices. To determine its properties, processing techniques and purity of metals are the main factors. Some prominent properties of metallic implants are their high yield strength, corrosion resistance, high tensile strength, resistance to fatigue and creep. They are usually used in orthopedic and dental application such as hip prothesis, knee prothesis, dental implants, etc. The most commonly used metals and alloys for these applications are stainless steels, commercially pure titanium and its alloys, and cobalt-based alloys. Fig. 2.2 shows that metallic implants for orthopedic applications.

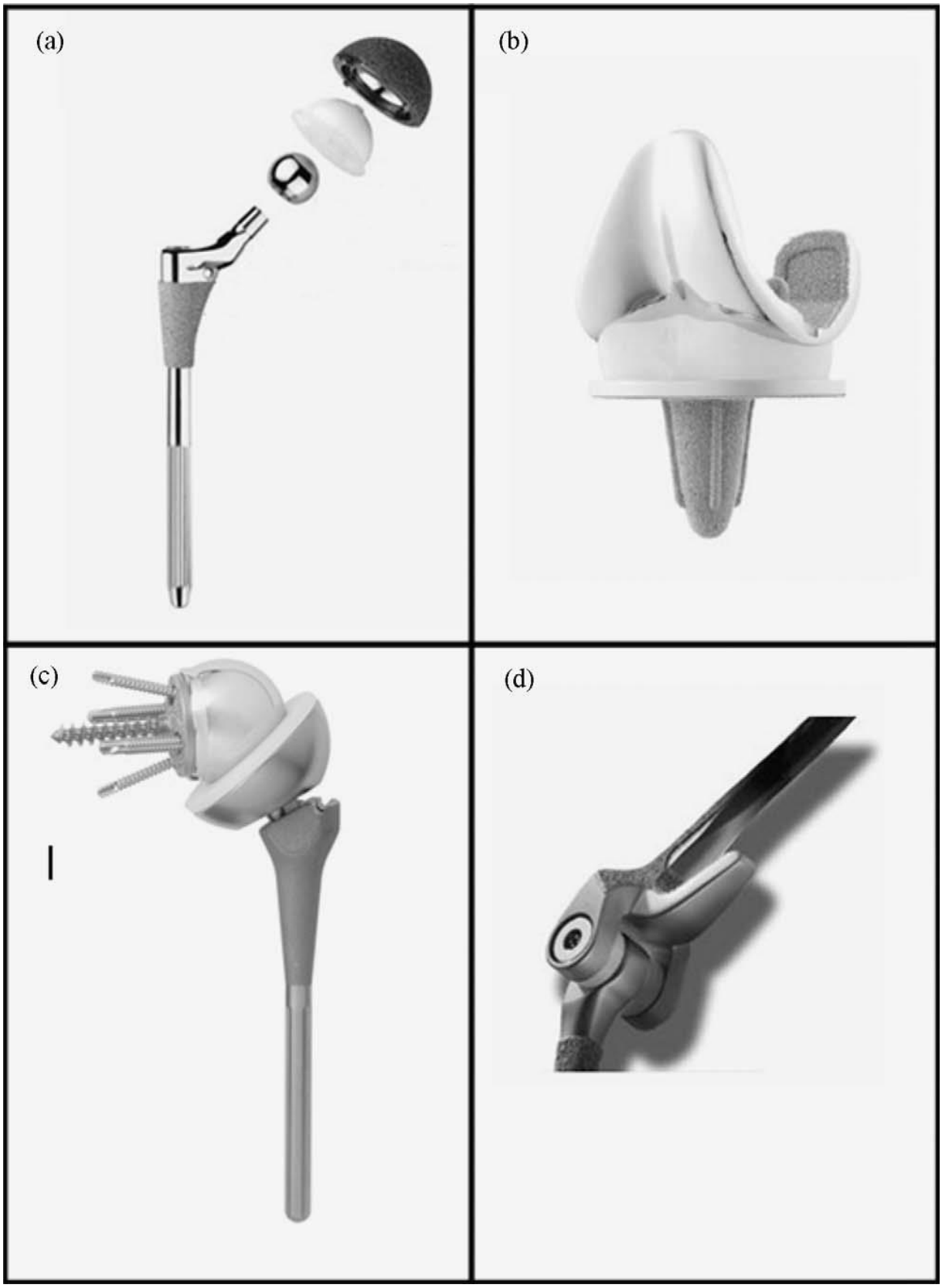

Figure 2.2 : Orthopedic implants used for load bearing systems: (a) hip prothesis, (b) knee implants, (c) shoulder implants, (d) elbow implants [22].

2.1.1.1 Stainless steels

Stainless steels (SS) are iron (Fe) based alloys with a minimum of 10.5% Cr as an alloying element. First stainless steel (18Cr–8Ni) implant was used in 1926 [23]. 316L (ASTM F128, F139), grade 2 is commonly used as an implant material. It is including 0.030% (wt. %) carbon for decreasing the probability of in vivo corrosion. The low ingredient of carbon "C" is symbolised by the presentation of "L". The iron (60-65%) content of 316L alloy is widely used as austenitic stainless steel with chromium (17-19%) and nickel (12-14%), in addition as a minor contents are nitrogen, manganese, molybdenum, phosphorous, silicon and sulfur. Following to molybdenum content, corrosion resistance is increased. By the decreasing the amount of C, which has low solid solubility range, at the grain boundary of chromium carbide ($Cr_{23}C_6$) is kept low and then, as a matter of fact improve corrosion resistance [24].

Lots of techniques such as vacuum arc melting and electro slag refinin are used in producing high quality stainless steels with minimum nonmetal additions for biomaterial applications [25]. For the processing of surgical, orthopedical or dental devices, several types of stainless steels (as shown in Table 2.2) are commonly used in these medical applications.

Table 2.2 : Several types of stainless steels in use for biomedical devices [20].

Types of stainless steels	Differences in Cr content (%)	Medical applications
Martensitic stainless steel	10.5-18	Dental burs, dental chisels, orthodontic pliers and scalpels
Ferritic stainless steel	11-30	Guide pins, fasteners
Austenitic stainless steel	16-26	Hip implants, knee implants, guide pins

2.1.1.2 Cobalt-chromium alloys

Cobalt (Co) based implant materials are commonly representatived as a Co-Cr alloys in biomedical applications. Co-Cr alloys were originallydeveloped for aircraft engines and heat-resistant materials. Co-Cr alloys exhibit significant mechanical properties such as corrosion resistance, strength and toughness, castability and wear resistance. Their corrosion resistance is better than stainless steel and their wear resistance is better than stainless steel and titanium alloys; but their plasticity and workability are lower than stainless steel and Ti alloys.

Cast Co-Cr-Mo alloys in use for biomedical applications are known as "Vitallium". Cast Co-Cr alloys have good resistance for the type of pitting and crevice corrosion. Generally, Co-Cr alloys have excellent wear resistance, hence they may be used for sliding parts of artificial joints. In the beginning, stents were made from a 40Co-20Cr-15Ni-7Mo-Mn alloy named "Elgiloy", which had been processed as a heat-resistant alloy, now stents are made from a stainless steel and Ni-Ti alloy. And at present 40Co-20Cr-15Ni-7Mo-Mn alloy is used for orthodontic arch wire [26].

2.1.1.3 Titanium and titanium alloys

First implanted titanium was used into laboratory animals in 1940 by Bothe, Beaton and Davenport. The conclusion of their work exhibit that the titanium was well-tolerated material comparative with stainless steel and Co-Cr-based alloys under in vivo conditions. The two most commercially specifications for titanium implants are pure Ti and Ti-6Al-4V. Commercially pure titanium may be chosen when the corrosion resistance is a principal importance than its mechanical properties. Ti-6Al-4V is an alpha-beta alloy, the microstructure of Ti-6Al-4V shows in Figure 2.3 to exhibit effects of different temperature [27].

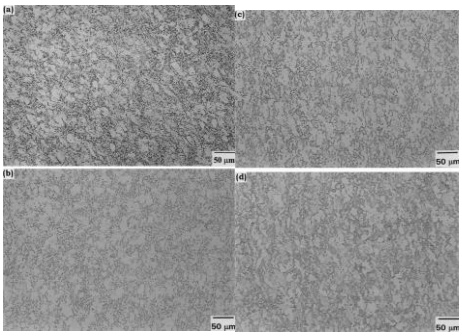

Figure 2.3 : Microstructure of Ti-6Al-4V samples were deformed in different temperature: (a) 750°C; (b) 800°C; (c) 850°C; (d) 900°C [27].

Table 2.3 : Ti-based metallic biomaterials mechanical properties and clinical applications [28].

Types of Ti alloys	Elastic modulus (GPa)	0.2% offset yield strength (MPa)	Ultimate tensile strangth	Elongation	Clinical applications
Pure Ti	102-110	170-480	240-550	15-24	Dental implants, maxillofacial and craniofacial implants
Ti6Al4V	110	860	930	10-15	Total joint replacement arthroplasty principal for hips and knees
Ti6Al7Nb	105	795	860	10	Femoral hip stems, fracture fixation plates, spinal components, nails, screws and wire
Ti13Nb13Zr	79-84	836-908	973-1037	10-16	Orthopedic implants

2.1.2 Ceramics

Ceramics, glasses and glass-ceramics are inorganic compounds of metallic or nonmetallic materials, with interatomic bonding as ionic or covalent and which are commonly formed at raised temperature. Ceramics are widely used in dentistry as restorative materials such as in gold-porcelain crowns, glass-filled ionomer cements, and dentures [29]. The succesfull ceramics are able to cause bone regeneration and bone in growth at the tissue-implant interface without the intermediate fibrous tissue layer.

Generally, any material is suitable for all biomedical applications. Ceramics, glasses and glass-ceramics are widely used to repair or replace skeletal hard connective tissues. The mechanism of tissue attachment is relevant the type of tissue response at the implant-tissue interface. There are four types of tissue response as shown in Table 2.4.

Table 2.4 : The type of materials and tissue response [29].

Material type	Tissue response
Toxic	The surrounding tissue dies
Nontoxic, bioinert	Fibrous tissue of different thickness forms
Nontoxic, bioactive	Interfacial bond forms
Nontoxic, biodegradable	Ths surrounding tissue replaces

2.1.3 Polymers

Polymers may be described as long chain molecules which are consisting of a number of small repeating units (monomers). Polymers are related to family of macromolecules and exhibit the biggest class of biomaterials. They can be processed not only from natural sources but also from synthetic organic sources. Variety types of polymers are listed in Table 2.5 [30].

Table 2.5 : Polymers used for biomedical applications [30].

Applications	Polymer
Orthopedic implants	Ultrahigh-molecular-weight-polyethylene
Finger joints	Silicone
Sutures	Polylactic and polyglycolic acid
Tracheal tubes	Silicone, acrylic, nylon
Heart pacemaker	Acetal, polyethylene, polyurethane
Blood vessels	Polyester, polytetrafluroethylene, PVC
Gastrointestinal segments	Nylon, PVC, silicones
Facial protheses	Polydimethyl siloxane, polyurethane, PVC
Bone cement	Polymethylmethacrylate

Polymers have some advantages for used as biomaterials:

- Easy to fabricate with different shapes and structures

- Provide broad range of bulk compositions and physical properties
- Can be easily tuned

Their disadvantages:

- Under in vivo condition, may penetrate some toxic compounds to the body
- Low mechanical strength
- Easy to absorb water and biomolecule and surface chemistry may be changed [28].

2.1.4 Composites

The meaning of composite is "consisting of two or more distinct parts." At the molecular and structural level, tissues such as bone and tendon are certainly composites with a number of levels of hierarchy. Used as biomaterial, composites are always designed to exhibit excellent mechanial properties and also biological compatibility.

Composites can be described based on the matrix material or on the bioactivity of the composites. There are three types of biomedical composites:

- Polymer matrix composites, e.g., carbon/PEEK
- Metal matrix composites, e.g., HA/Ti, HA/Ti-6Al-4V
- Ceramic matrix composites, e.g., stainless steel/HA, glass/HA

Showing regard to bioactivity of the composites, there are three different types of biomedical composites:

- Bioinert composites, e.g., carbon/carbon, carbon/PEEK.
- Bioactive composites, e.g., stainless steel/bioglass, HA/HDPE, HA/Ti-6Al-4V
- Bioresorbable composites, e.g., tricalcium phosphate (TCP)/polylactic acid (PLA) [31].

2.2 Performance Factors of Biomaterials

Solid materials shows different kinds of properties such as mechanical, chemical, electrical, optical, thermal or magnetic. In the biomedical application, the three properties are highly important as follow:

- Mechanical Properties
- Corrosion Behavior
- Biocompatibility

2.2.1 Mechnical properties

The most important properties of materials which are used in medicine and denstistry are the mechanical properties. In engineering, mechanical properties such as elastic, tough, ductility have important meanings to describe qualitative explanation of materials. These quantitative descriptions will be depended on stresses and strains. Materials impose upon mechanical deformation, the *stress* is explained as a force or load per unit area, which is mostly represented in Newtons per square meter (Pascal, PA) or pounds force per square inch (psi):

$$\text{Stress } (\sigma) = \frac{\text{force}}{(\text{cross - sectional area})} \cdot \left[\frac{\text{N}}{\text{m}^2}\right] \tag{2.1}$$

The *strain* is defined as the deformation of a material in response to an applied load.

$$\text{Strain } (\varepsilon) = \frac{\text{deformed length - original length}}{\text{original length}} \left[\frac{\text{m}}{\text{m}}\right] \text{or} \left[\frac{\text{in}}{\text{in}}\right] \tag{2.2}$$

This is fundamentally the equation used for nonrigid materials like polymers and soft tissues. For rigid materials such as metals, ceramics and hard tissue (bone) inflection are highly small and the more sensitive method is needed.

As shown in Figure 2.4, the normalized load (force/area) is stress (σ) and the normalized deformation (change in lenght/original lenght) is strain (ε).

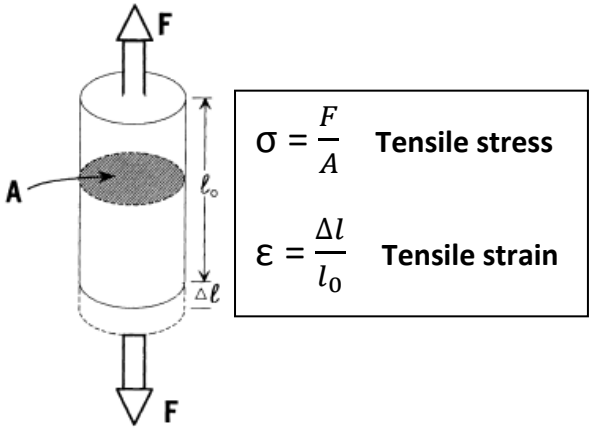

Figure 2.4 : Tensile stress and strain [32].

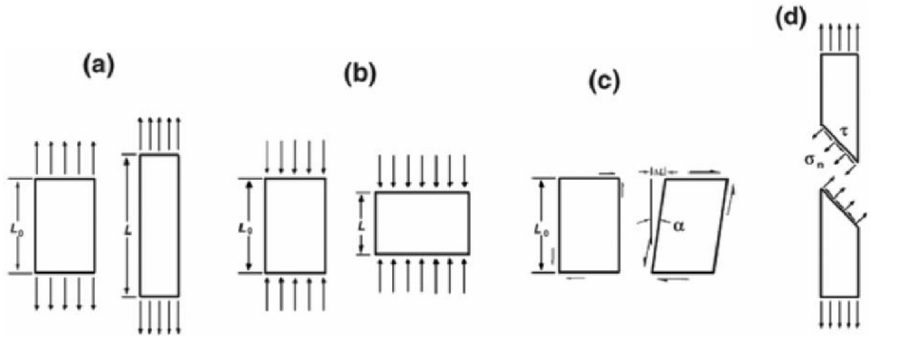

Figure 2.5 : Three types of deformation: (a) tension, (b) compression, (c) shear, and (d) shear in tension. Tension and compression produce the shear stresses as in (d) [33].

The deformation related with different types of stresses are defined as tensile, compressive and shear strain.

The stress-strain behavior of a material is plotted on a graph, a curve shows a continuos response of an idealized material in the direction of the exposed force can be acquired, as seen in Figure 2.5. The yield point (σ_y or YP) can separate the stress-strain curve of solid into elastic and plastic region.

In the elastic region, the strain and stress increase in the direct proportion.

$$\text{Hooke's law: } \sigma = E\varepsilon, \text{ tension or compression} \tag{2.3}$$

$$\tau = G\gamma, \text{ shear.} \tag{2.4}$$

Table 2.6 : Some mechanical properties of metallic materials, tissue and polymer [32].

	Elastic modulus	Yield strength (MPa)	Tensile strength (MPa)	Elongation to failure (%)
CoCr Alloy[a]	225	525	735	10
Ti6Al4V	120	830	900	18
Bone (cortical)	15 to 30	30 to 70	70 to 150	0-8
Polyethylene	0.4	-	30	15-100

[a] 28% Cr, 2% Ni, 7% Mo, 0.3% C (max.), Co balance.

E, the tensile constant or Young's modulus and G, is the shear modulus. For materials, which have strong bonds (e.g., diamond, tungsten), these Young's modulus and shear modulus are high and when the stress is given, it produces a very small strain [34]. Elastic modulus of some important biomaterials are showed in Table 2.6.

2.2.2 Corrosion resistance

Materials have differences corresponding to their chemical composition, structure, impurities and surface condition. Corrosion is a chemical process in opposition to mechanical wear; the loss of the surface is not a result of the abrasion of metallic particles, but is based on the transformation of metal atoms which are from the metallic to the non-metallic condition of chemical compounds or dissolved ions [35].

Corrosion of implant materials or metallic biomaterials induces the damage of their structural unity and surface function. It gives accelaration their fatigue and wear, on the other side, such damage gives accelaration the corrosion. Corrosion mechanisms of implants can induce change to bioenviroments, such as alteration in pH, decrease of dissolved oxygen, alteration in chemical compouns and so on. Further, quite few amount of released metal ions may cause cytotoxic or allergic response in the living tissue [36].

It is clear that to note down and clarify all relevant things of corrosion is possible just in a few cases. Hereby, corrosion estimations are mostly with regard to merely supposal [37]. The statistics show that controlling corrosion is a big problem and there is no trivial task. It is predicted that the cost relevant corrison in the western industrial countries amount to 3-5% of the gross national product, only 25% of it can be described avoidable by way of known precautions [38,39].

Even though corrosion can be defined into lots of different types, all corrosion effects in aqueous solutions are with regard to two essential reactions:

1. They occur in anaerobis conditions and water is the oxidation agent. Hydroxides, hydrated oxides or metal oxides can be formed in this following equation:

$$Me + n \bullet H_2O \Longleftrightarrow Me(OH)_n + n/2 \bullet H_2 \qquad (2.5)$$

2. When oxygen is the oxidation agent, it occurs under aerobic conditions. Metal oxides, hydroxides or hydrated oxides are formed, but the reaction occurs without the formation of hydrogen. The equation is as follow:

$$Me + n \bullet H_2O + n/2 \bullet O_2 \Longleftrightarrow Me(OH)_n \qquad (2.6)$$

To continue the total electrical neutrality, anodic and cathodic reactions must advance in balance during the corrosion mechanism. Various types of corrosion may occur on metallic implant materials are galvanic, intergranular, pitting, stress-corrosion cracking, corrosion fatigue and fretting. Figure 2.6 shows the optical micrographs to exhibit the formation of pitting corrosion in biomaterial grade AISI 316L stainless steel following immersion in the different types of simulated body fluids (SBF) [40].

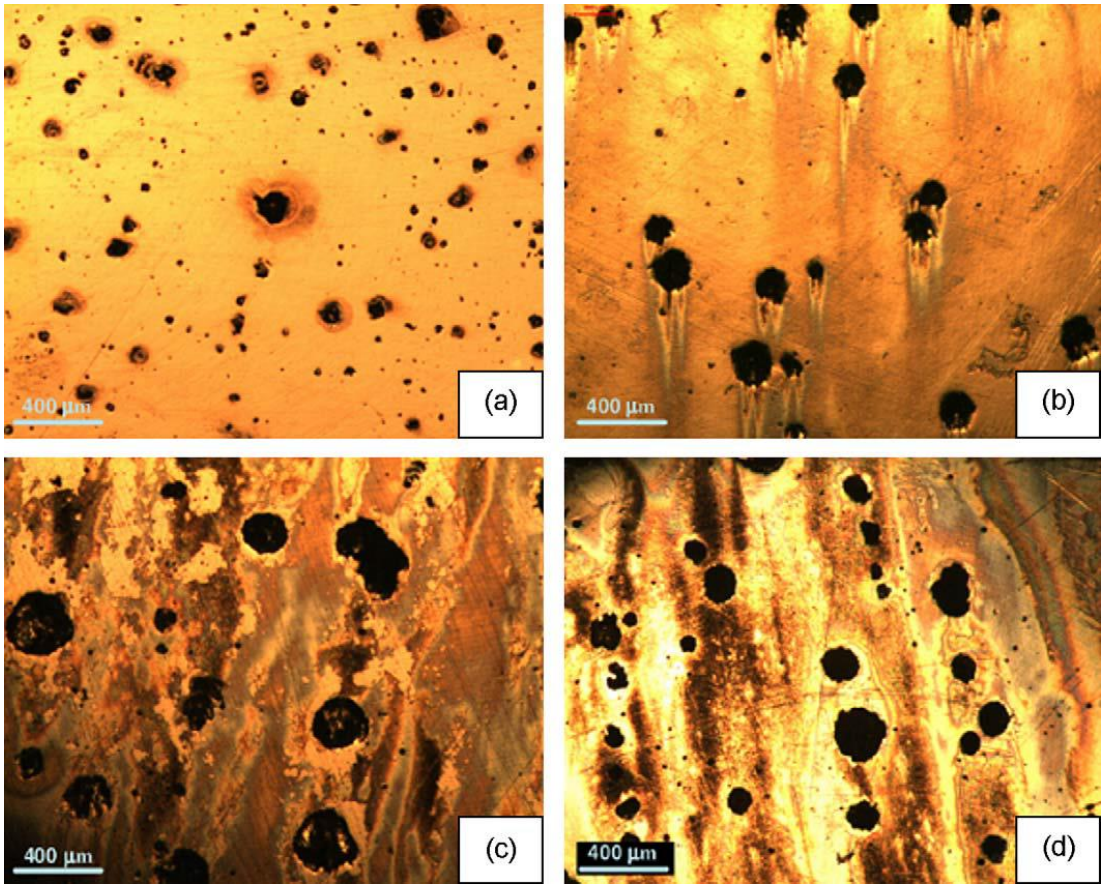

Figure 2.6 : Optical micrographs exhibit the formation of pitting corrosion in medical application of grade AISI 316L stainless steel immersion in (a) NaCl, (b) NaCl + albumin, (c) phosphate buffered solution (PBS) and (d) PBS +albumin [40].

The principles of different types of corrosion and their applications in bioenvironment are greatly explained in lots of earlier publications [41, 42, 43].

2.2.3 Biocompatibility

The producer of biomaterials should prove that the product is safe, not cytotoxic or not allergenic and will perform the role as intended. Performance and safety of biomaterials are principal, usually described by the term biocompatibility. Biocompatibility may be explained as "the adoption of the implant material by the surrounding tissues without any unfavorable response from the body and vice versa" [42]. Biocompatibility is related to the interactions that take place between biomaterials and host tissue. Consequently, a biocompatible implants should be nontoxic, nonallergenic, noncarcinogenic, without any undesirable body reaction and be chemically stable or corrosion resistant. Figure 2.7 shows that if three important factors (patient, material, material function) change, biocompatibility can change.

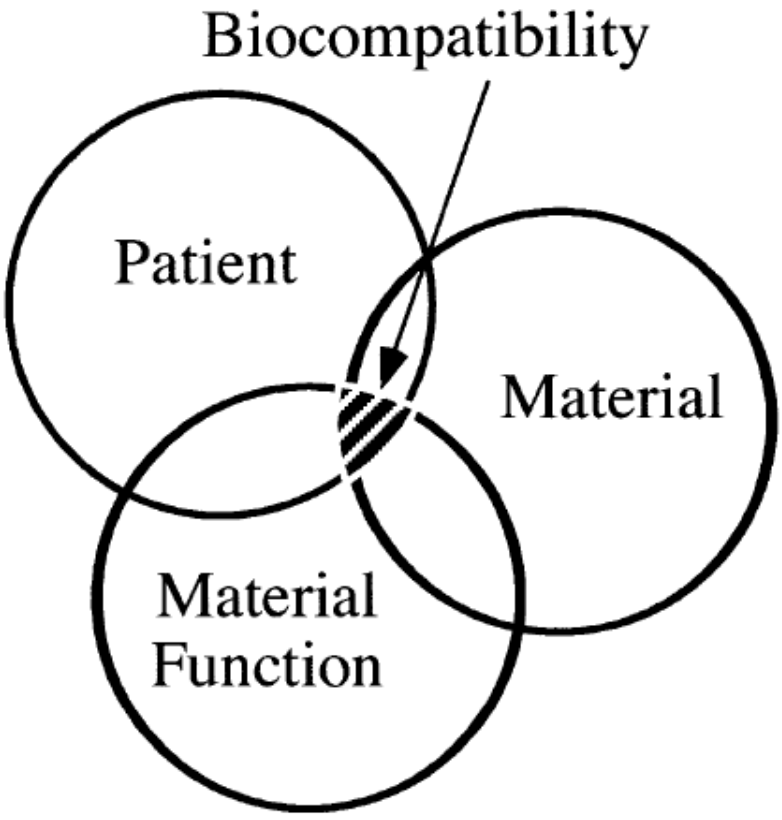

Figure 2.7 : Interactions between host, material, and application of material are important in biocompatibility [44].

Some calcium phosphate salts found in bone are brushite ($CaHPO_4•2H_2O$), octacalcium phosphate ($Ca_8H_2[PO_4]_6•5H_2O$), and calcium hydroxyapatite ($Ca_{10}[PO_4]_6•5H2O$). But hydroxyapatite (HA) is the raid lattice structure of hard tissue. Consequently, using synthetically reproduced HA may be an excellent interest to regenarate bone for failures.

Ca – P containing biocompatible implant surface can be fabricated using calcium phosphate salts (as shown in Table 2.6), with $1 \leq Ca/P \leq 2$ are not encapsulated by a fibrous tissue and allows for bone in growth to the implant surface [43].

Table 2.7 : Formula, mineral name, and various Ca/P ratio of Ca-P based ceramic [24].

Ca-P	Formula	Name/Mineral	Abbreviation
1.0	$CaHPO_4•2H_2O$	Hydrated calcium phosphate/Brushite	DCP
1.0	$CaHPO_4$	Anhydrous calcium phosphate/Monetite	ADCP
1.33	$Ca_8H_2(PO_4)_6•5H_2O$	Octacalcium phosphate	OCP
1.55	$Ca_3(PO_4)_2$	Tricalcium phosphate/ Whitlockite	TCP
1.67	$Ca_{10}(PO_4)_6•F_2$	Flourapatite	FA
1.67	$Ca_{10}(PO_4)_6(OH)_2$	Hydroxylapatite	HA
2.0	$CaO•Ca_3(PO_4)_2$	Tetracalcium phosphate/ Hilgenstockite	TTCP

Various works have demonstrated the bioactivity and biocompatibility of such salts [44]. Detsch et al. showed the response of osteoclast-like cells on sintered tricalciumphosphate (TCP) and hydroxyapatite (HA). This work exhibited that osteoclast-like U-937 cells responded in a different form to HA and TCP (as shown in Figure 2.8) [45]. Detsch et al., consequently, suggested that Ca-P based ceramics as a bone representative material must be chosen either for their fast degradation (TCP) or for the slow The authors, therefore, proposed that calcium phosphate-based ceramics as a bone substitute material must be chosen either for their fast degradation (TCP) or for the slow transforming of the biomaterial (HA). The chosen type of ceramic depends on the location and size of the bone defect and the patient's personal characteristics.

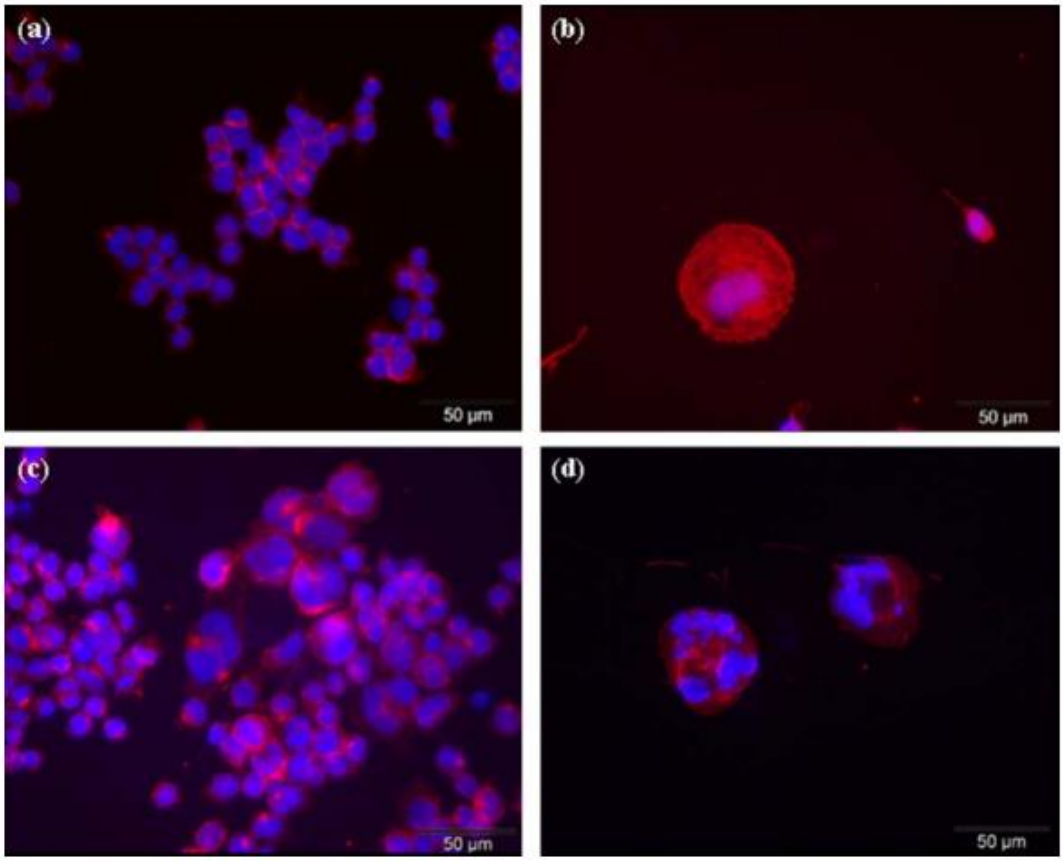

Figure 2.8 : Fluorescence microscopy images of U-937 cells cultured on (a and b) TCP, and (c and d) HA, after 21 days [44].

3. EXPERIMENTS

The aim of the present study is to evaluate the bone tissue response to Ca-P apatite modified titanium (Ti) based implants. Bioactive layers were grown by a micro arc oxidation (MAO) process. The type of samples which were subjected to the MAO were classified with respect to the antibacterial agents including Zinc and Copper. In the present study, commercial purity CpTi and titanium alloy (Ti6Al4V represented as 64) and were utilized as a substrate and represented as CpTi, CpTi-MAO, 64, 64-MAO. Zn-doped samples were represented as CpTi-MAO-Zn, 64-MAO-Zn. Cu-doped samples were represented as CpTi-MAO-Cu, 64-MAO-Cu.

3.1 Preparation of Ti Samples

Commercially pure titanium discs (CpTi, Grade 4) and titanium alloy (Ti6Al4V) with size of 10 mm in diameter, 4 mm in length were used. Samples were polished with following series silicon carbide papers of No. 320, 600, 1200 and 2500 grit and ultrasonic cleaned with 100% ethanol, asetone and last deionized water for 15 min.

3.2 Surface Treatments

The titanium discs were generally divided into 2 groups depends on a basement type: CpTi (commercially pure titanium) and 64 (Ti6Al4V). CpTi-MAO and 64-MAO were subjected to MAO with an applied positive voltage of 440 V and negative voltage of 80 V in an electrolyte (Electrolyte 1) containing calcium acetate hydrate (VWR BDH Prolabo) and sodium phosphate (Alfa Aesar) and 2 liter distilled water during the 5 minutes. CpTi-MAO-Zn and 64-MAO-Zn were modified with an electrolyte (Electrolyte 2) containing calcium acetate and sodium phosphate, zinc acetate dihydrate (Alfa Aesar) and 2 liter distille water during the 5 minutes. Other groups were prepared with same conditions but only copper acetate were used as an antibacterial agent source (Electrolyte 3). Table 4.1 shows electrolytes and amounts of chemicals. The pulse frequency and duty cycle were 500 Hz and 60%,

respectively. During processing, variation of current density and applied voltage was continuously recorded with a sampling time of 750 ms by using a memory recorder system (Hioki, Memory Hicorder 8808). Each sample was oxidized for 5 min and then cleaned in distilled water.

Table 3.1 : Types of electrolyte and amounts of chemicals.

Electrolyte	Amounts of Chemicals
Electrolyte 1	• Sodium phosphate: 14.4 g/L • Calcium acetate: 41 g/L • 2 L distilled water
Electrolyte 2	• Sodium phosphate: 14.4 g /L • Calcium acetate: 41 g/L • Zinc acetate: 10.974 g/L • 2 L distilled water
Electrolyte 3	• Sodium phosphate: 14.4 g /L • Calcium acetate: 41 g/L • Copper acetate: 9.98 g/L • 2 L distilled water

These three different electrolytes effected the macro and microstructures of samples. All samples included Ca-P apatite bioactive layer, barely some of them included Zn and Cu on surface and also into the layers.

3.3 Surface Characterization

Surface properties, i.e. chemical composition, surface thickness, morphology/pore characteristics, crystal structure, roughness, surface wettability were characterized with various analytical techniques.

The morphology and mean elemental composition of the MAO exposed surfaces were evaluated by utilizing scanning electron microscopes (SEM, Jeol JSM-6510 and Jeol NeoScope JCM- 6000, FEI Nova Nanosem 450, FEI Nova Nanolab 600) equipped with energy dispersive spectrometers (EDS). The thicknesses and compositions of the oxide layers were determined during SEM and electrone probe micro-analyzer (EPMA, JXA-8530F) examination by imaging the cross-sections of the samples after gentle grinding and polishing. The phase composition of the coatings was identified by conducting X-ray diffraction (XRD, GBC, MMA 027 and Seifert 3003 T/T) analysis using Cu-Kα radiation at 35 kV and 28.5 mA. Scan range was between 10–90° and scanning speed was 2°/min at a scan step of 0.020°. The average surface roughness (Ra) of the samples was measured by using a surface profilometer (Veeco Dectac, 6M) under 5 mg load, with a scan distance of 2000 μm and scan duration of 30 sec. Surface wettability (contact angle measurement) was carried out by static drop method (KSV Cam 200).

3.4 Ion Releasing Test

Inductively coupled plasma optical emission spectrometry (ICP-OES) analysis revealed the release of Zn and Cu ions from the Zn, Cu-incorporated samples into the simulated body fluid (SBF) and ultra pure water (MQ). Simulated body fluid was prepared according to 1x Tas SBF protocol. 1x Tas SBF was shown in Table 3.2. [1] Ion releasing experiment set up as below;

Figure 3.1 : Ion releasing test time chart.

Figure 3.2 : Shaking bath for ion releasing test.

As shown in Fig. 3.2, each time samples were withdrawn from the 20 mL SBF solution and put the fresh SBF. During the release times, samples were waited in shaking bath (as shown in Fig. 4.2) with the conditions 50 rpm, 37ºC. 1 mL zinc containing SBF solution was dissolved in 1 mL HNO3 and then diluted 10 times and the amount of zinc released were measured by ICP-OES.

Table 3.2 : 1x Tas SBF contents and amounts of them [45].

Contents	Amounts of chemicals
Deionized water	960 mL
NaCl	6.5456 g
$NaHCO_3$	2.2682 g
KCl	0.373 g
Na_2HPO_4	0.1419 g
$MgCl_2 \times 6H_2O$	0.3049 g
1 M HCl	9 mL
$CaCl_2 \times 2H_2O$	0.3675 g
Na_2SO_4	0.071 g
Tris[= $(CH_2OH)_3CNH_2$]	6.057 g
1 M HCl	30 mL

Total volume was 1000 mL and pH was 7.41, temperature was 37°C.

.

4. RESULTS

In this present work, pure titanium (CpTi) and titanium alloy (Ti6Al4V, represented as 64) were used as a basement. Crystal structure, surface examinations, surface roughness and wettability, scartch test, ion releasing results were seperated as CpTi-based samples and Ti6Al4V-based samples this thesis.

4.1 CpTi-based Samples

CpTi-based samples were representatived as CpTi, CpTi-MAO, CpTi-MAO-Zn, CpTi-MAO-Cu.

4.1.1 Crystal structure analysis

The XRD patterns of the CpTi-MAO and the CpTi-MAO-Zn and the CpTi-MAO-Cu were shown below. Normally, CpTi revealed the presence of the α-titanium peaks only because the structure of material is a α-titanium. MAO treated Ti indicated the presence of anatase and rutile TiO_2 crystalline phases.

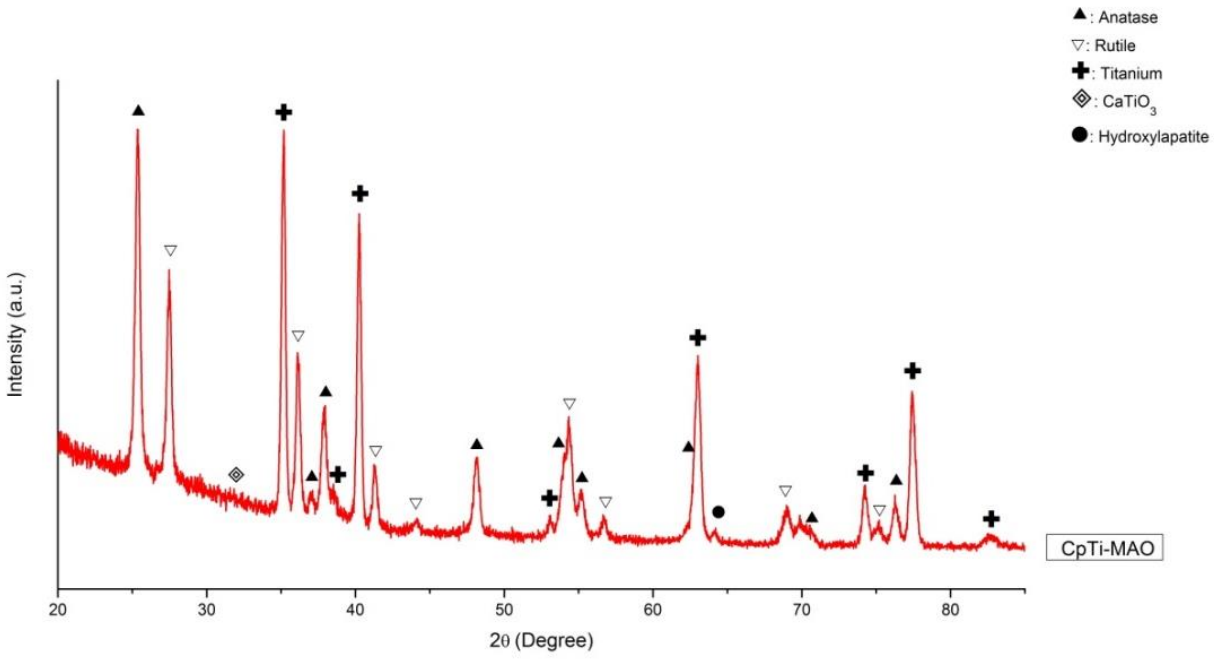

Figure 4.1 : XRD spectra of the CpTi-MAO.

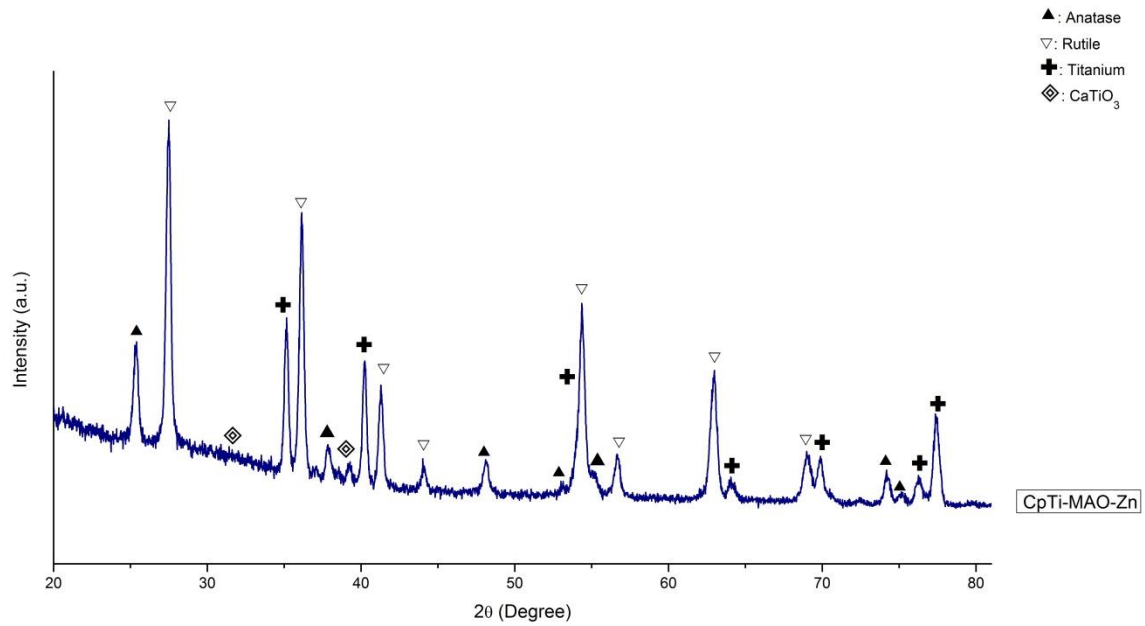

Figure 4.2 : XRD spectra of the CpTi-MAO-Zn.

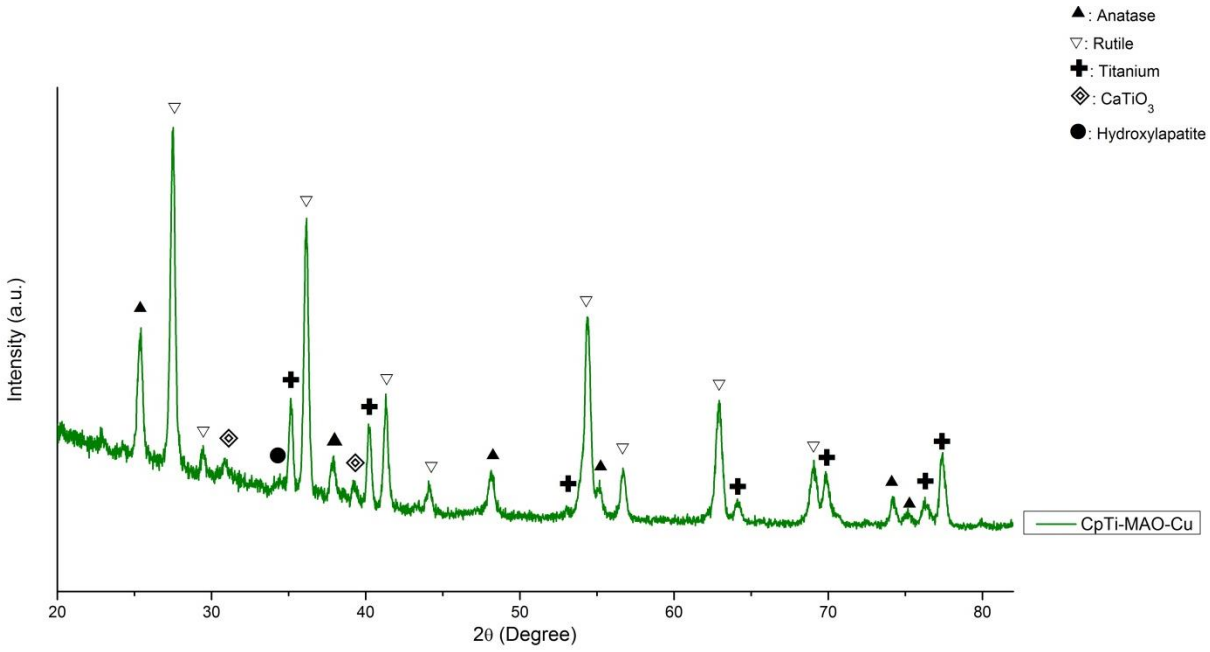

Figure 4.3 : XRD spectra of the CpTi-MAO-Cu.

ThisFig 4.1 was shown the XRD pattern of the CpTi-MAO sample. MAO treated Ti indicated the presence of anatase and rutile TiO_2 crystalline phases. The rutile phase in the oxide layer means that MAO coating has a stable structure. The XRD patterns of the CpTi-MAO showed a few notable differences especially on the intensity of phases. As Fig. 4.2 was shown that the CpTi-MAO-Zn sample, due to incorporation of Zn affected the intensity of major peaks such as rutile, anatase and α-Ti.

4.1.2 Surface examinations

CpTi samples were characterized as macroscopical (as shown in Fig. 4.4, Fig. 4.5). In Fig. 4.4 macro view of CpTi-MAO had high whiteness rating than macro view of CpTi-MAO-Zn. Ca-P deposition rate differences may cause color differences regarding to EDS result of CpTi-based samples.

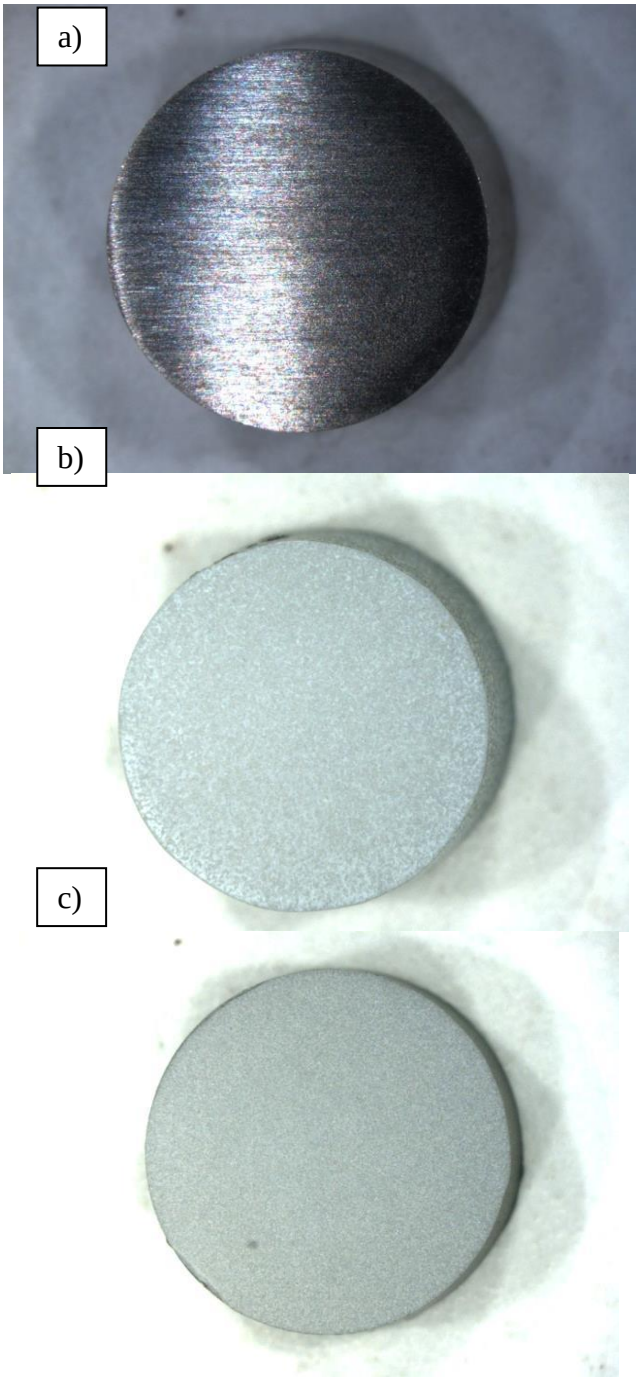

Figure 4.4 : a) Uncoated CpTi, b)CpTi-MAO, c)CpTi-MAO-Zn.

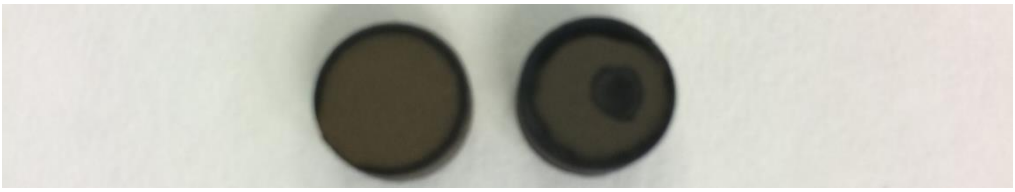

Figure 4.5 : CpTi-MAO-Cu samples.

The macro view of CpTi-MAO was exhibited white colour comparision in the view of CpTi-MAO-Cu. In Fig. 4.5 shown that CpTi-MAO-Cu exhibited black colour.

CpTi-MAO			**CpTi-MAO-Zn**		
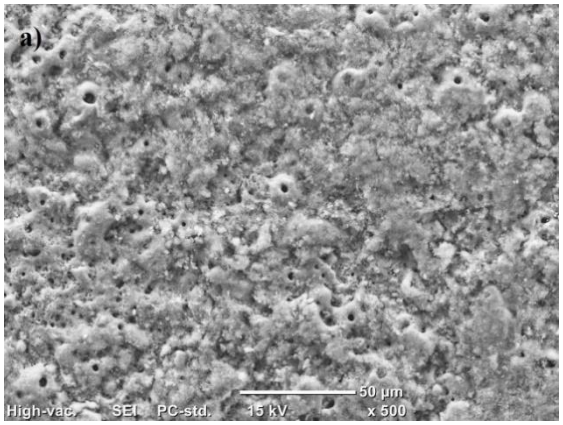			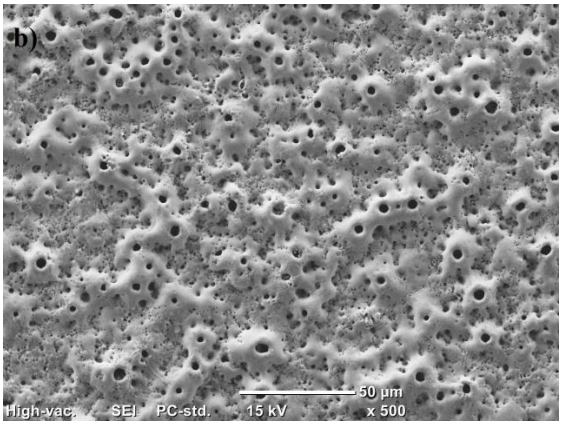		
Element	**wt.%**	**Atom%**	**Element**	**wt.%**	**at.%**
Titanium	22.32	10.38	Titanium	39.26	19.80
Oxygen	53.92	75.09	Oxygen	49.07	74.08
Phosphorus	8.08	5.81	Phosphorus	1.21	0.94
Calcium	15.67	8.71	Calcium	5.64	3.40
-	-	-	Zinc	4.82	1.78

Figure 4.6 : Morphology and composition of Ti surfaces: SEM micrographs showing a) CpTi-MAO and b) CpTi-MAO-Zn surface morphology, EDS results showing composition of the samples.

Figure 4.6 shows SEM images and EDS results of the coated Ti surfaces. Anodic oxidation has been demostrated to be a suitable technique to produce a porous surface with topographic features. CpTi-MAO and CpTi-MAO-Zn exhibit porous surface, the pore size and the distance between neighbor pores are clearly different. The porosity of CpTi-MAO was seem lower than CpTi-MAO-Zn. Besides, the associated EDS spectra of the CpTi-MAO and the CpTi-MAO-Zn showed that the deposition of Ca and P which generated biocompatible compounds. The atomic ratios of Ca and P are considered Ca/P ratio was calculated as 1.49 and 3.61 for the CpTi-MAO and the CpTi-MAO-Zn samples. Differently from the surface of the CpTi-MAO sample, the surface of the CpTi-MAO-Zn sample was also enriched by Zn (4.82 wt.%) owing to the incorporation of Zn from the electrolyte.

CpTi-MAO-Cu

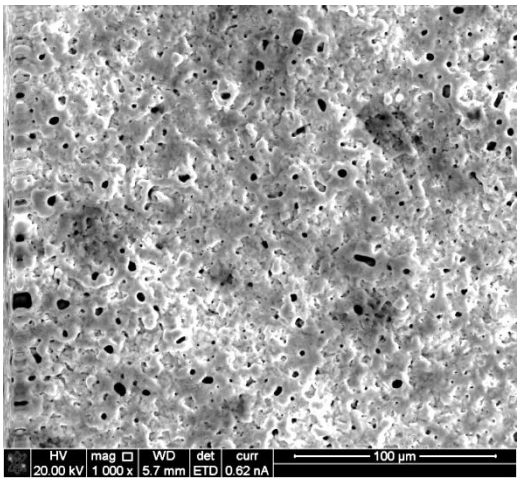

Element	wt.%	at.%
Titanium	37.72	18.88
Oxygen	48.81	73.15
Phosphorus	2.98	2.31
Calcium	7.61	4.55
Copper	2,43	0,92

Figure 4.7 : Morphology and composition of Ti surface: SEM micrographs showing CpTi-MAO-Cu surface morphology, EDS results showing composition of the sample.

Figure 4.7 shows SEM image and EDS result of the coated Ti surface. Anodic oxidation has been demostrated to be a suitable technique to produce a porous Cu-incorporated surface with topographic features as Zn-incorporated sample. CpTi-MAO-Cu exhibited porous surface, the pore size and the distance between neighbor pores are clearly different than Zn-incorporated sample. Besides, the associated EDS spectra of the CpTi-MAO-Cu showed that the deposition of Ca and P which generated biocompatible compounds. The atomic ratios of Ca and P are considered Ca/P ratio was calculated as 1.96 and 3.61 for the CpTi-MAO-Cu and the CpTi-MAO-Zn samples. CpTi-MAO-Cu sample exhibited more apatite-like morphology than Zn-doped sample. Differently from the surface of the CpTi-MAO sample, the surface of the CpTi-MAO-Cu sample was also enriched by Cu (2.43 wt.%) owing to the incorporation of Cu from the electrolyte.

On the other hand, the pore sizes of Zn-doped samples showed in Fig. 4.8. Micro and nano pores were observed and the average micro pore size was calculated as ≈ 5.28 μm and nano pore size as ≈ 232 nm.

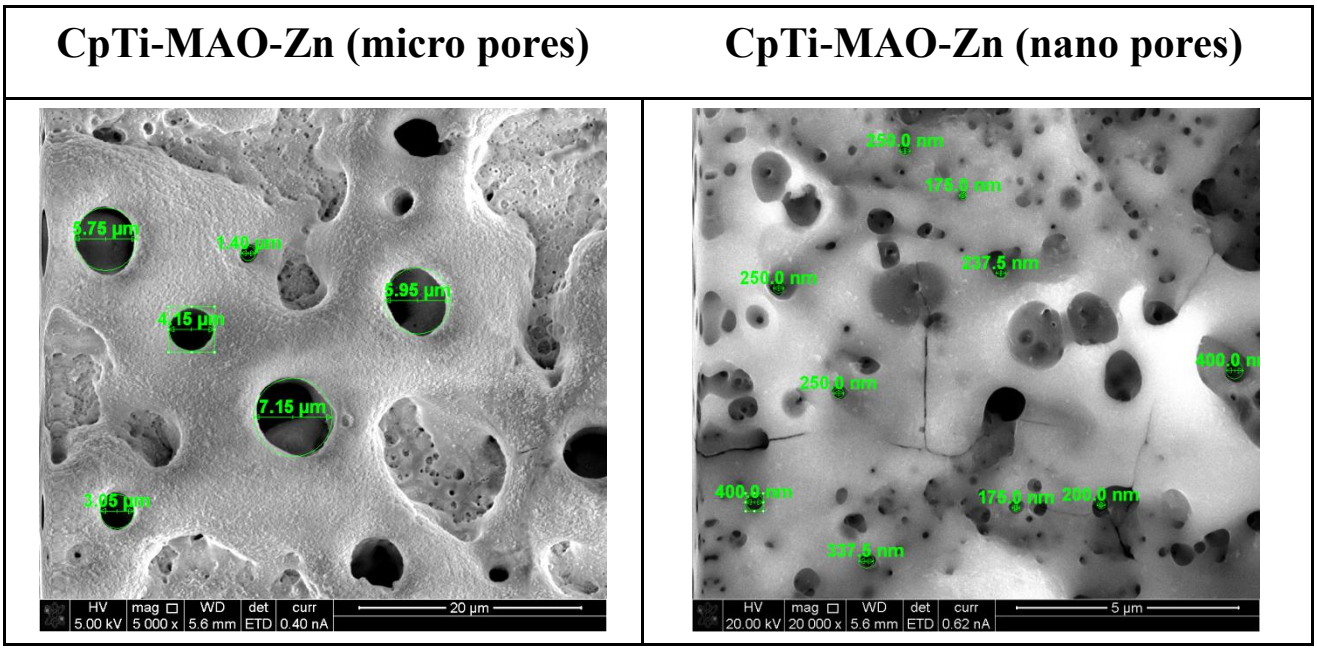

Figure 4.8 : The micro and nano pore sizes of CpTi-MAO-Zn samples.

The thickness of the biocompatible compound layers were shown in Fig. 4.9 as below. TiO_2 layers having thicknesses of 778.8 nm for the CpTi-MAO sample and 893.9 nm for the CpTi-MAO-Zn sample were observed beneath the biocompatible compound layers. Ca-P containing biocompatible layers were different thickness for each samples. CpTi-MAO was ≈ 5.5 μm and CpTi-MAO-Zn was ≈ 8.63 μm.

CpTi-MAO	CpTi-MAO-Zn
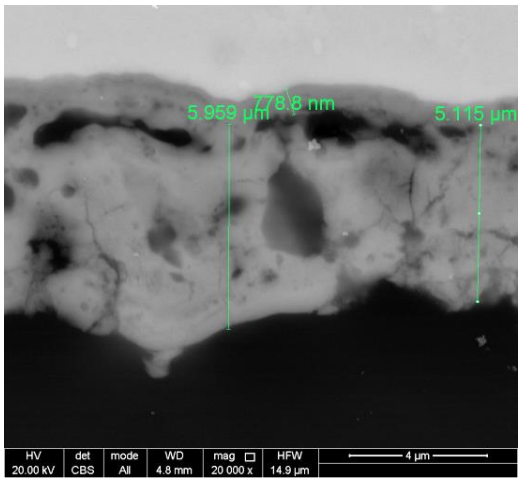	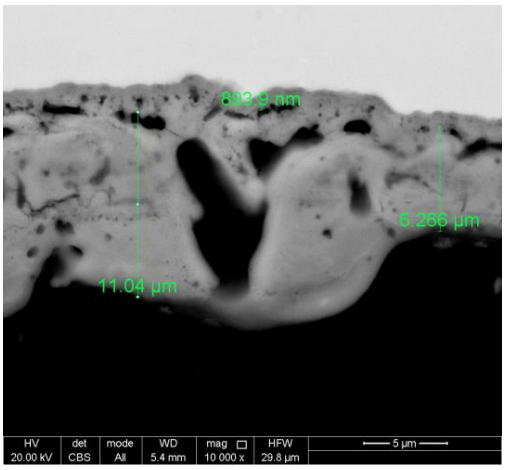

Figure 4.9 : The thickness of MAO coated Ti disc and MAO coated Zn-doped Ti disc.

CpTi-MAO-Cu
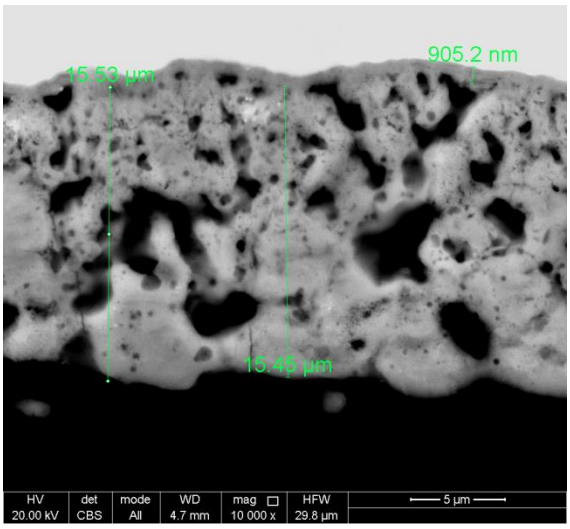

Figure 4.10 : The thickness of MAO coated Cu-doped Ti disc.

The thickness of the biocompatible compound layer was shown in Fig. 4.10. TiO_2 layers having thicknesses of 905.2 nm for the CpTi-MAO-Cu sample was observed beneath the biocompatible compound layers. Ca-P containing biocompatible layer was ≈ 15.49 µm.

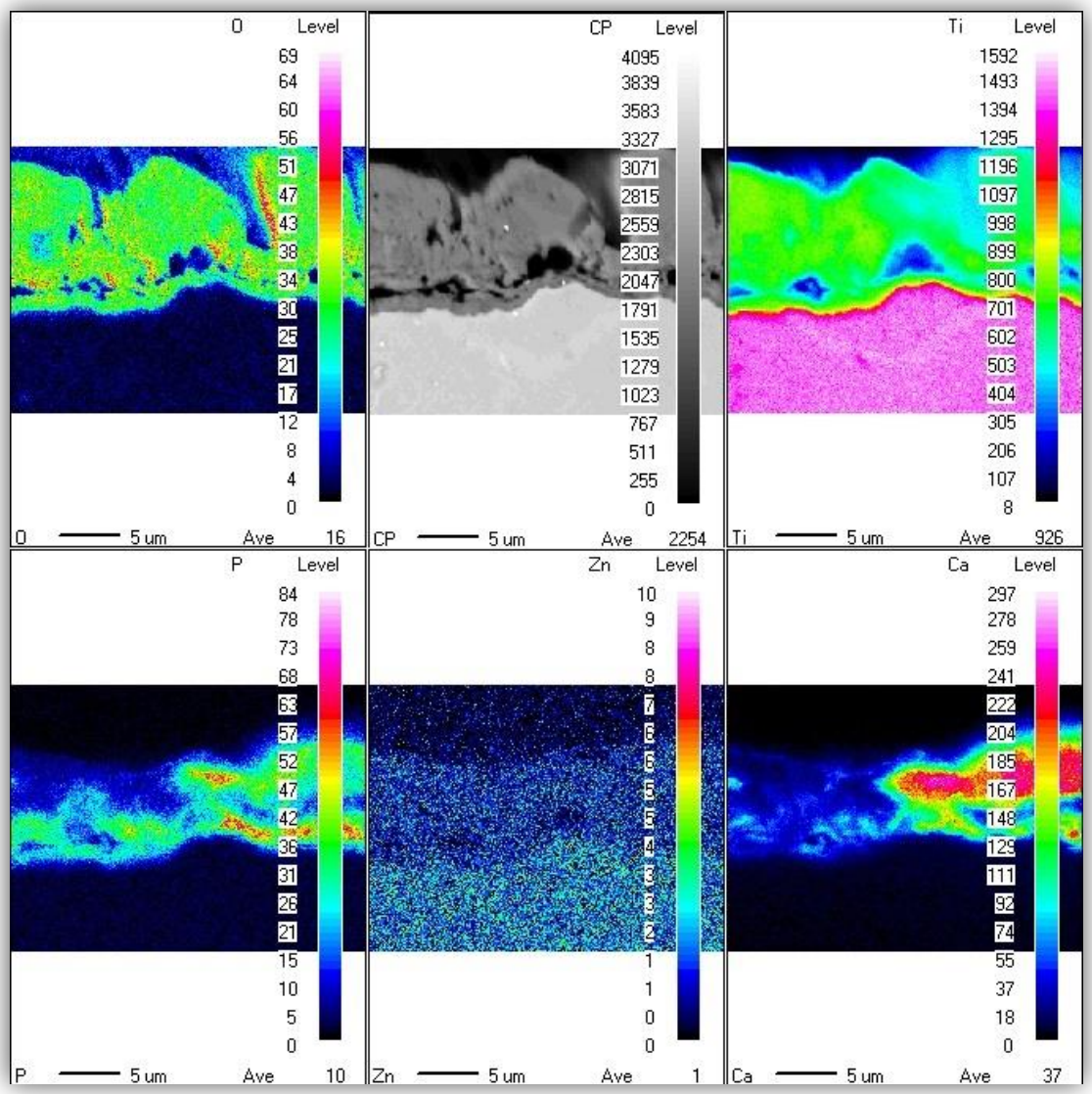

Figure 4.11 : The thickness of MAO coated Cu-doped Ti disc.

As shown in Fig. 4.11, it can be concluded that Ca and P were distributed over the inner layers of the sample. According to the EPMA result of CpTi-MAO, Ti and O were seemed in biocompatible compound layer. Ti showed downward high concentration because of the basement content.

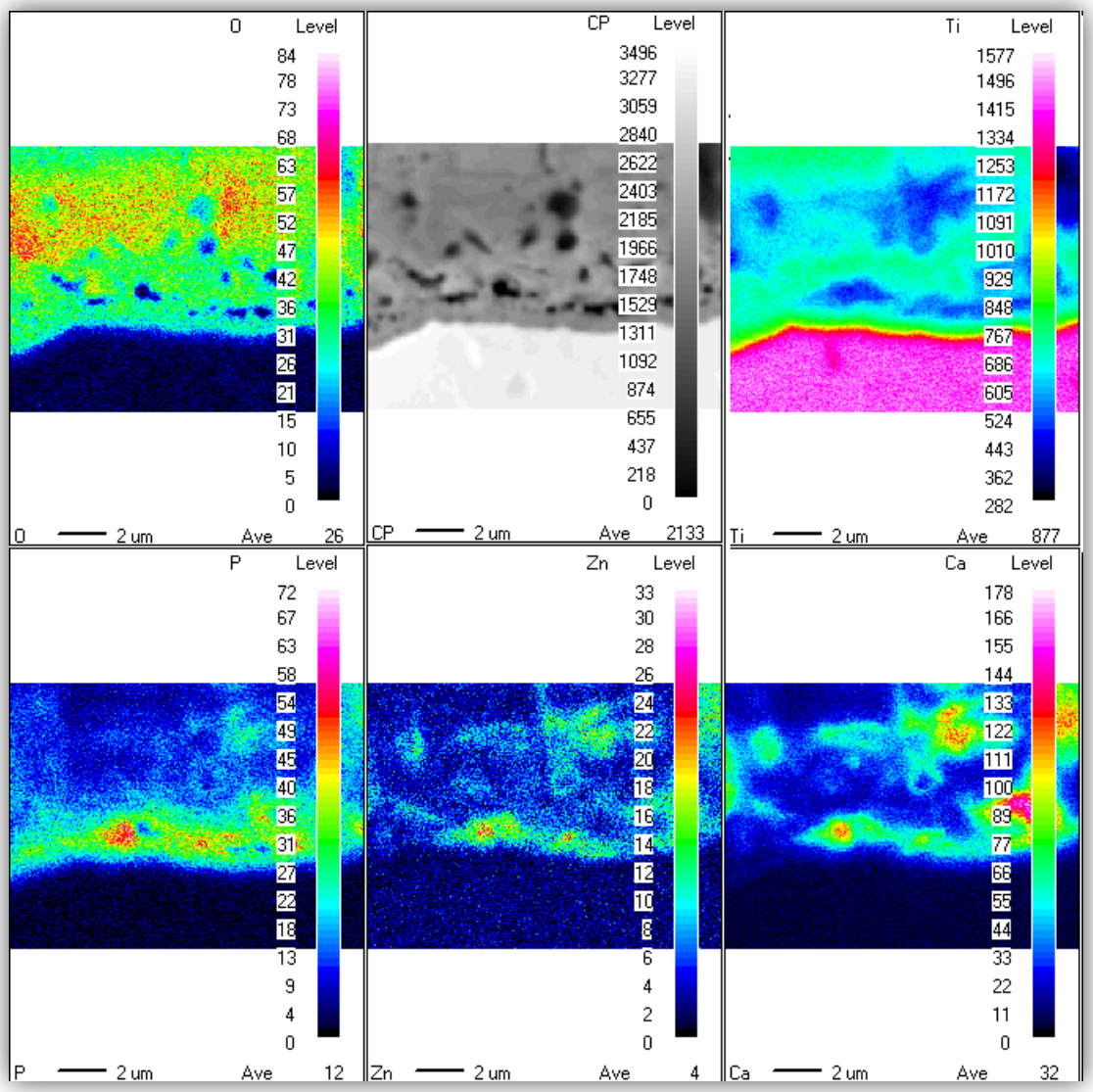

Figure 4.12 : The elemental mapping of CpTi-MAO-Zn.

EPMA mapping result of CpTi-MAO-Zn was shown in Fig. 4.12. It can be concluded that Ca, P and Zn were distributed over the inner layers of the sample. Ca, P and Zn were seemed closed each other. Zn was distributed inner layers, expecially closed to TiO_2 layer. Ti content decreased and when Ca, P, Zn contents increased.

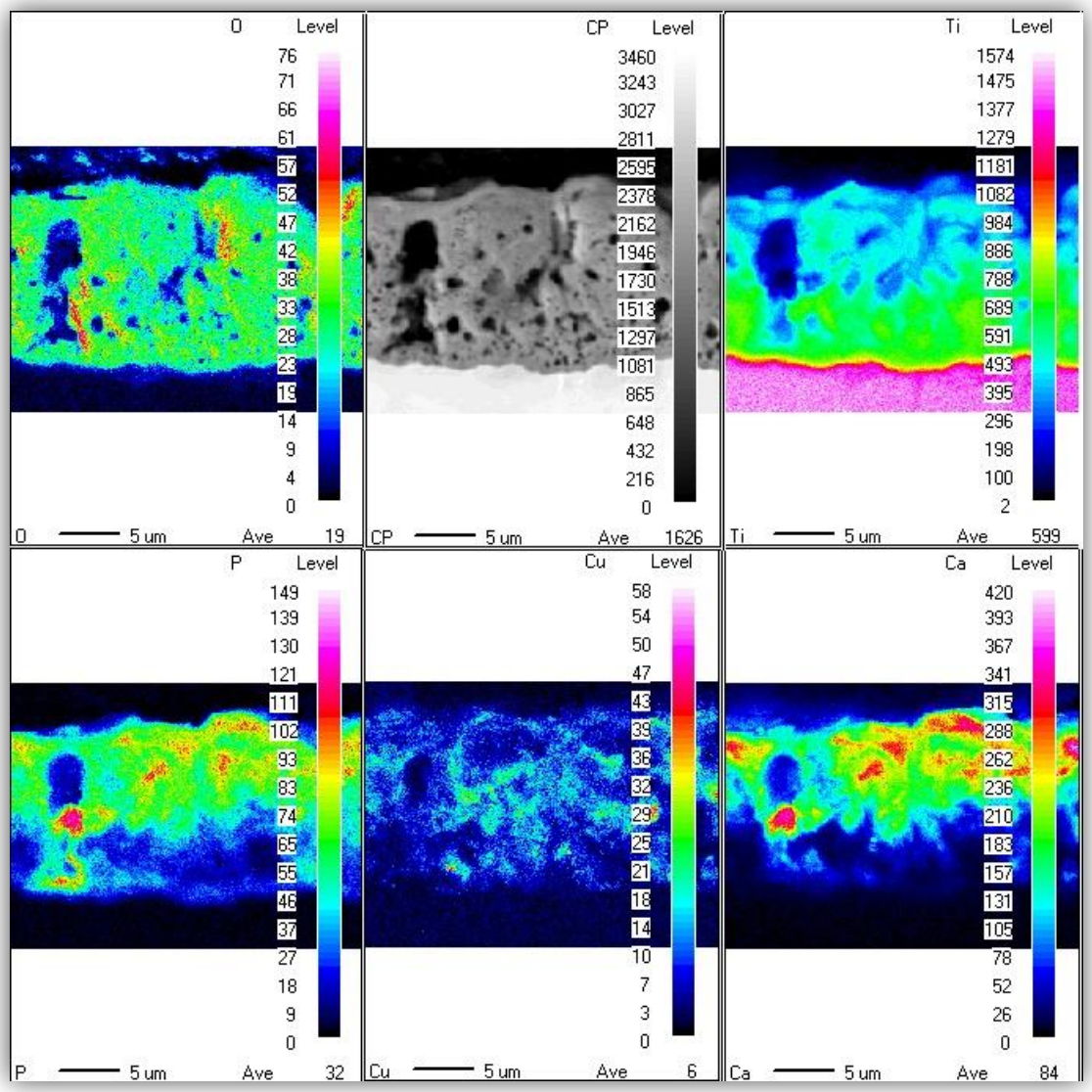

Figure 4.13 : The thickness of MAO coated Cu-doped Ti disc.

EPMA mapping result of CpTi-MAO-Cu was shown in Fig. 4.13. It can be concluded that Ca, P and Cu were distributed over the inner layers of the sample. Cu showed homogenous distribution through the inner layers. Ca, P exhibited highest dissociation in cross sectional sample of CpTi-MAO-Cu than cross sectional sample of CpTi-MAO-Zn.

4.1.3 Surface roughness and wettability

Surface roughness of two different samples (CpTi-MAO, CpTi-MAO-Zn) were measured, and they are shown in Fig. 4.14. The surface roughness of the CpTi-MAO appeared to be higher as compared to that in the CpTi-MAO-Zn. The Ra values for

the CpTi-MAO and CpTi-MAO-Zn surfaces were 1.743392 μm and 1.291863 μm, respectively.

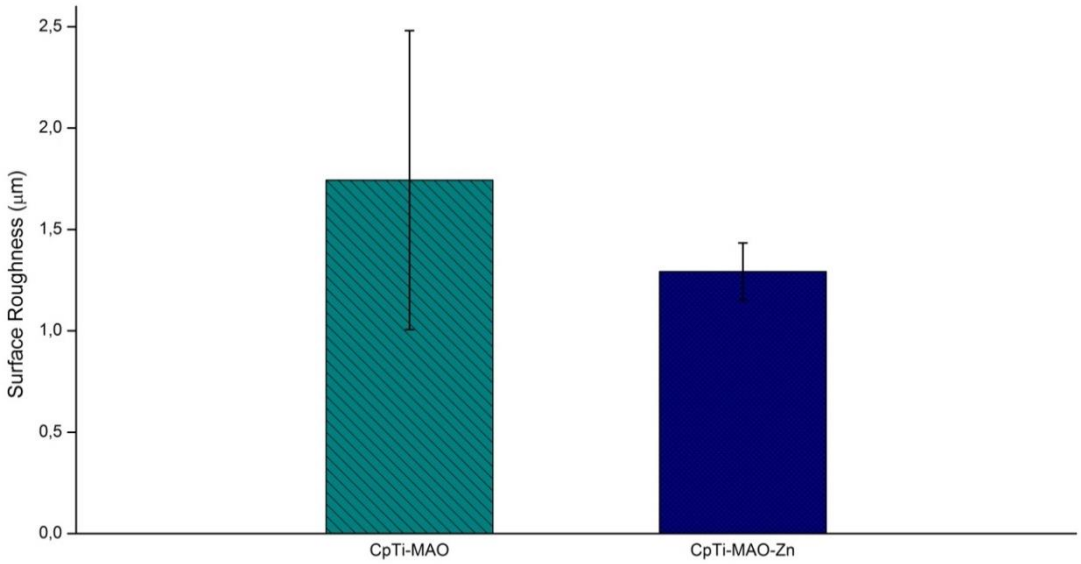

Figure 4.14 : Surface roughnesses of CpTi-MAO and CpTi-MAO-Zn.

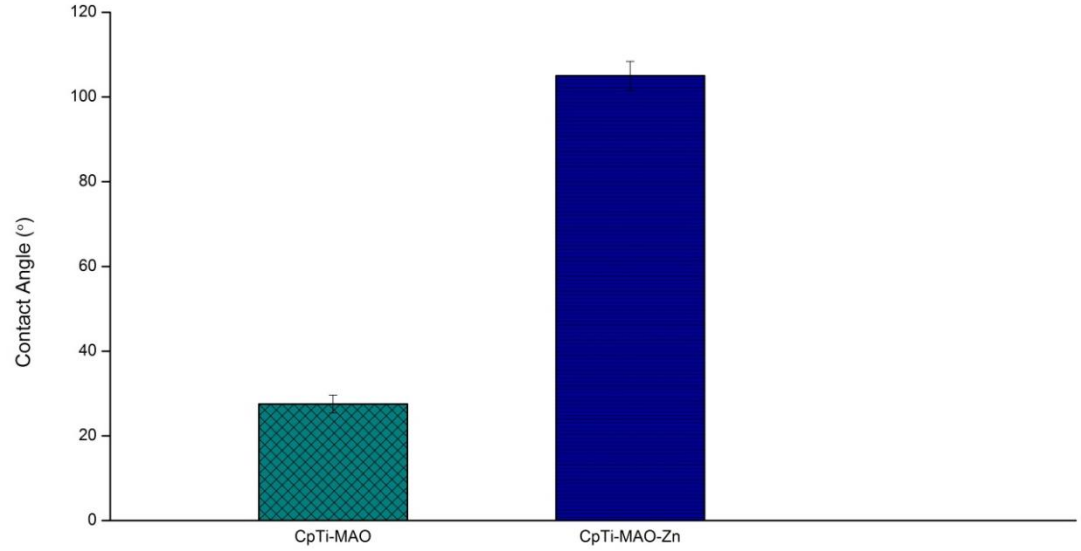

Figure 4.15 : Surface wettabilities of CpTi-MAO and CpTi-MAO-Zn.

Contact angle measurements are probably the most useful technique to measure the average wettability of a surface. The angle formed between the solid-liquid interface and liquid-vapor. The interfacial tensions of the solid-vapor (γ_{sv}) interface, liquid-vapor (γ_{lv}) and solid-liquid (γ_{sl}) interface, and the contact angle (Θ), are related by an equation known as the Young's equation.

$$\gamma_{lv} \cos\theta = \gamma_{sv} - \gamma_{sl} \quad (4.1)$$

If the contact angle is high (>90º) then the surface is considered as a hydrophobic surface. Surface wettability of two different samples (CpTi-MAO, CpTi-MAO-Zn) were measured, and they are shown in Fig. 4.15. The surface wettability of the CpTi-MAO appeared to be lower as compared to that in the CpTi-MAO-Zn. The contact angle values for the CpTi-MAO and CpTi-MAO-Zn surfaces were 27.52 º and 105.01º. It can be observed that Zn-incorporation can increase the hydrophobicity of the surface significantly.

4.1.4 Rockwell C Adhesion Tests

Mechanical properties of CpTi-MAO, CpTi-MAO-Zn surfaces were examined by Rockwell C adhesion tests. Rockwell C adhesion tests were conducted on the MAO layers using a Rockwell hardness tester (Zwick ZHR 4150). Rockwell C type diamond cone indenter penetrated into the layers with an applied load of 150 kg. After the Rockwell C adhesion tests, the surrounding area of indent was examined using an optical microscope (OM, Leica ICC50HD).

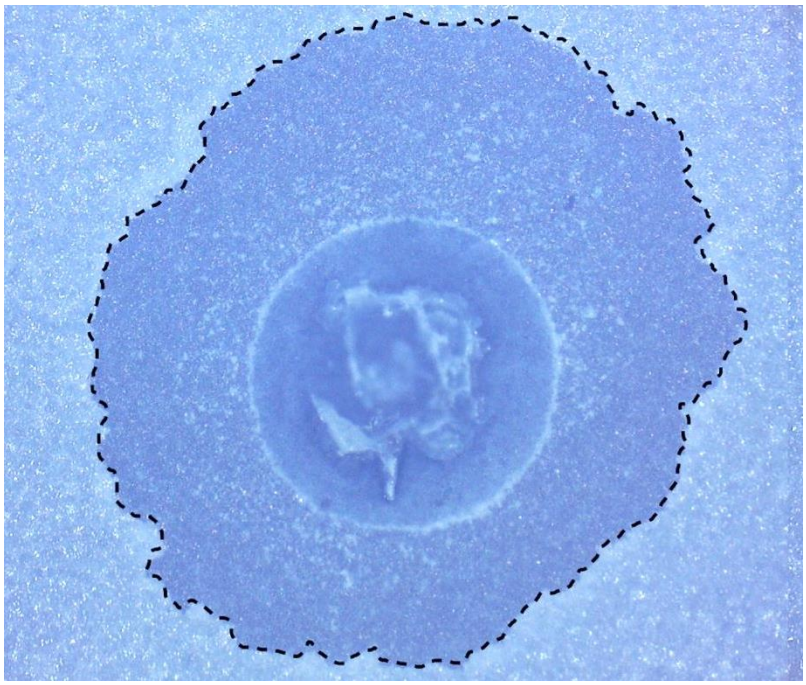

Figure 4.16 : The OM image showing periphery of indent (detached area is encircled) after Rockwell C adhesion test conducted for CpTi-MAO.

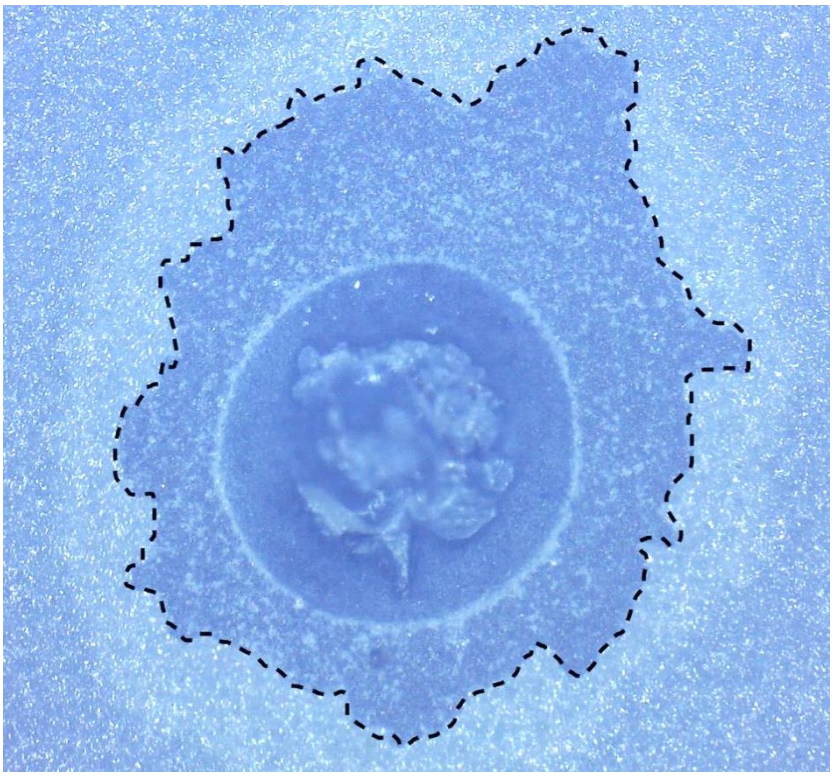

Figure 4.17 : The OM image showing periphery of indent (detached area is encircled) after Rockwell C adhesion test conducted for CpTi-MAO-Zn.

Results of the Rockwell C adhesion tests are presented as the OM images of the indents and their surroundings at 50X magnification in Fig. 4.16 and 4.17. Delamination zones were detected at the surroundings of the indents. Relatively smaller size of the delamination zone suggests better adhesion for the oxide layer of the CpTi-MAO-Zn sample as compared with that of the CpTi-MAO sample.

4.1.5 Ion releasing

Ion releasing from the CpTi-MAO-Zn and CpTi-MAO-Cu were investigated by ICP-OES. The release of Zn and Cu ions from the samples into the simulated body fluid (SBF) showed in Fig. 4.18, into the MQ showed in Fig. 4.19.

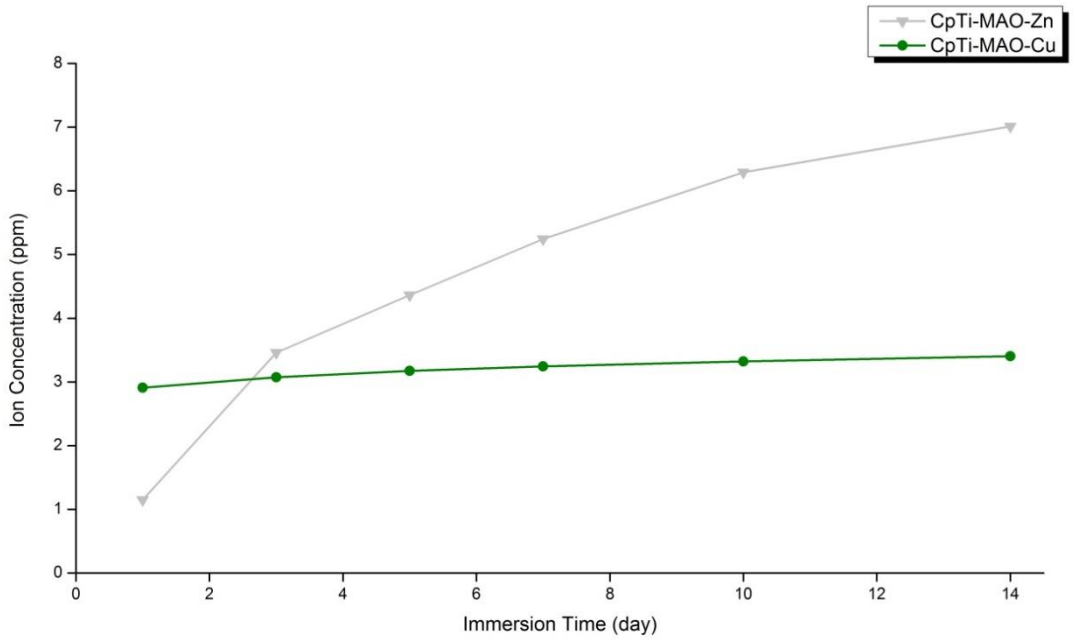

Figure 4.18 : The ion concentrations (Zn, Cu) into the SBF.

After 14 days, Zn ions were measured and totally 7.001 ppm Zn ions released into the SBF. Cu ions released lower than Zn ions and totally 3.4046 ppm Cu ions released into the SBF. Literature reported that zinc ion concentration of 10 µg/ml (=10 ppm) in the complete cell medium could induce 50% cell death._According to this information, Zn ions will be not affected as cytotoxic for human cells [46].

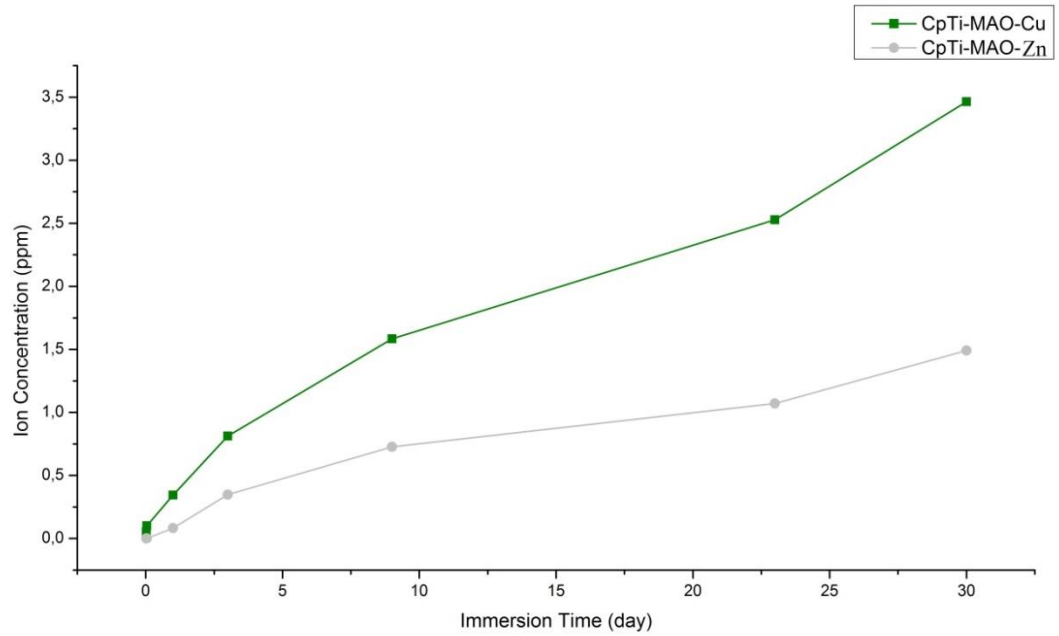

Figure 4.19 : The ion concentrations (Zn, Cu) into the MQ.

After one month into the ultra pure water, Cu ions released higher than Zn ions and totally Cu ions was measured as 3.4635 ppm. Zn ions were measured as 1.491 ppm.

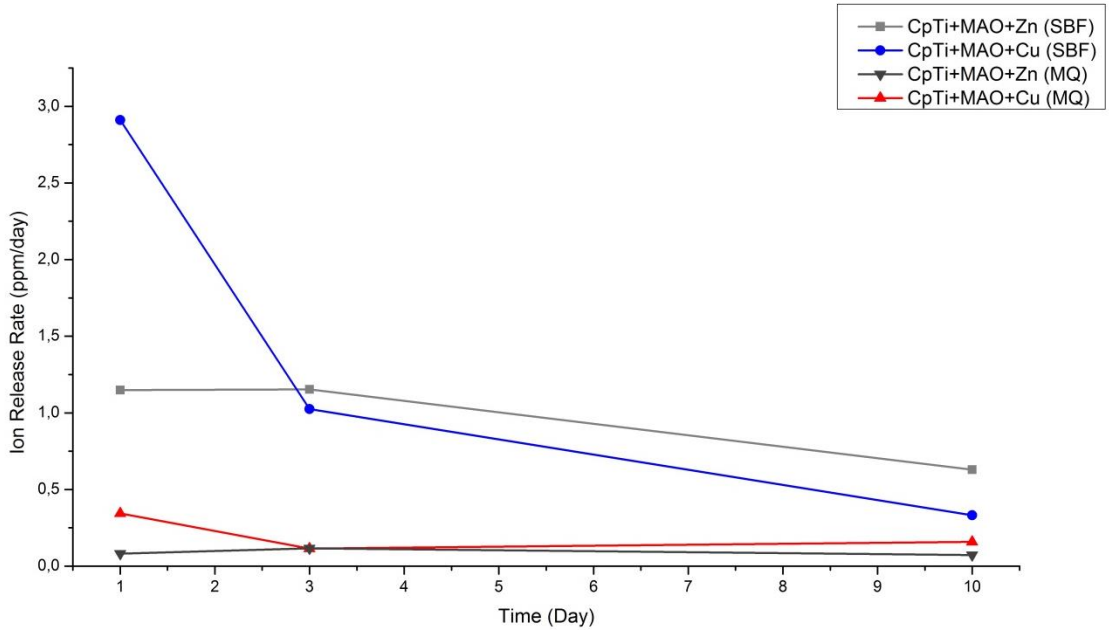

Figure 4.20 : Ion release rate for CpTi-MAO-Zn, CpTi-MAO-Cu into SBF and MQ.

In Fig. 4.20 shows ion release amount per day into SBF and MQ. CpTi-MAO-Cu showed highest releasing amount than CpTi-MAO-Zn into SBF at the first day. Into MQ, Cu-incorporated samples showed high release amount than Zn-incorporated at the first day. After 10 days, CpTi-MAO-Zn showed highest release rate into SBF.

4.2 Ti6Al4V-based Samples

Ti6Al4V-based samples were representatived as 64, 64-MAO, 64-MAO-Zn.

4.2.1 Crystal structure analysis

The XRD patterns of the 64-MAO and the 64-MAO-Zn were shown below. Normally, Ti6Al4V revealed the presence of the α-titanium peaks and β-titanium because the structure of material.

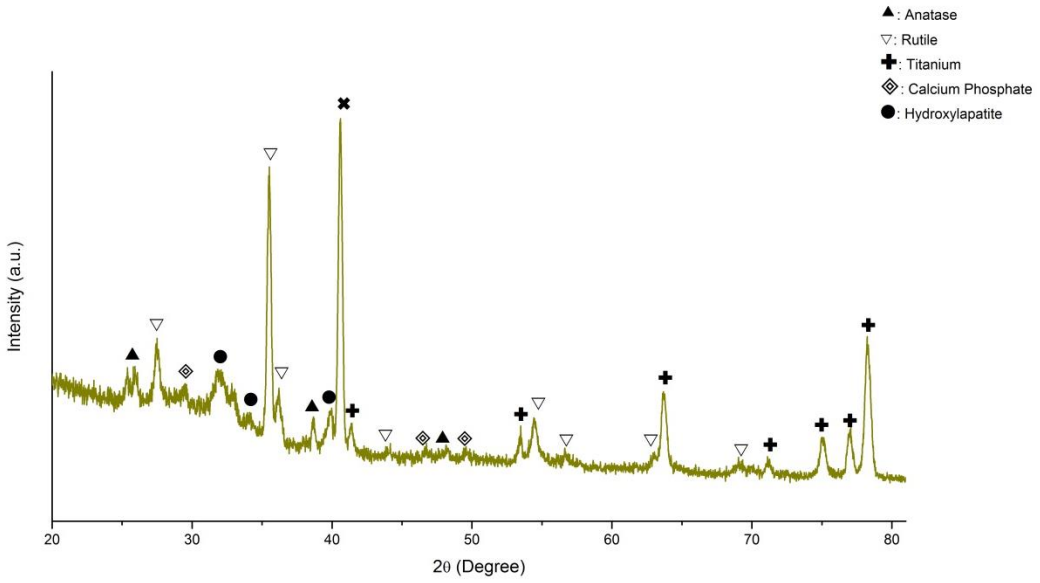

Figure 4.21 : XRD spectra of the 64-MAO.

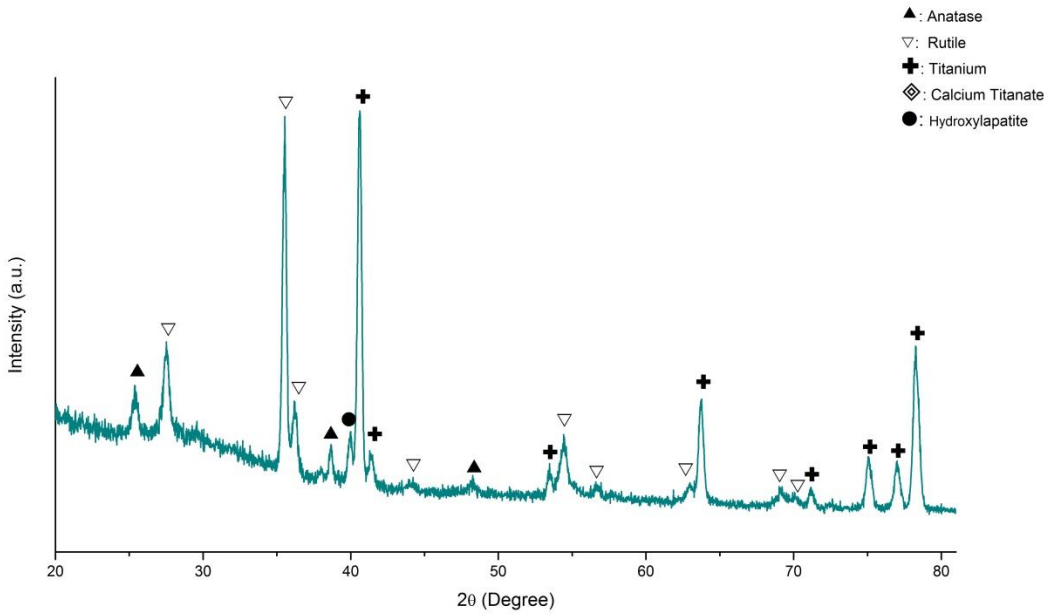

Figure 4.22 : XRD spectra of the 64-MAO-Zn.

Fig 4.21 and 4.22 were shown the XRD patterns of the both 64-MAO and Zn-doped sample representative as 64-MAO-Zn. MAO treated Ti6Al4V indicated the presence of anatase ($TiO_{2)}$ as a minor oxide phase, rutile and titanium as major phases in 64-MAO. As Fig. 4.22 was shown that the 64-MAO-Zn sample, due to incorporation of Zn affected the intensity of major and minor phases such as rutile, anatase and titanium.

4.2.2 Surface examinations

Ti6Al4V samples were characterized as macroscopical (as shown in Fig. 4.23). In Fig. 4.23 macro view of 64-MAO had high whiteness rating than macro view of 64-MAO-Zn. Ca-P deposition rate differences may cause color differences regarding to EDS result of 64-based samples.

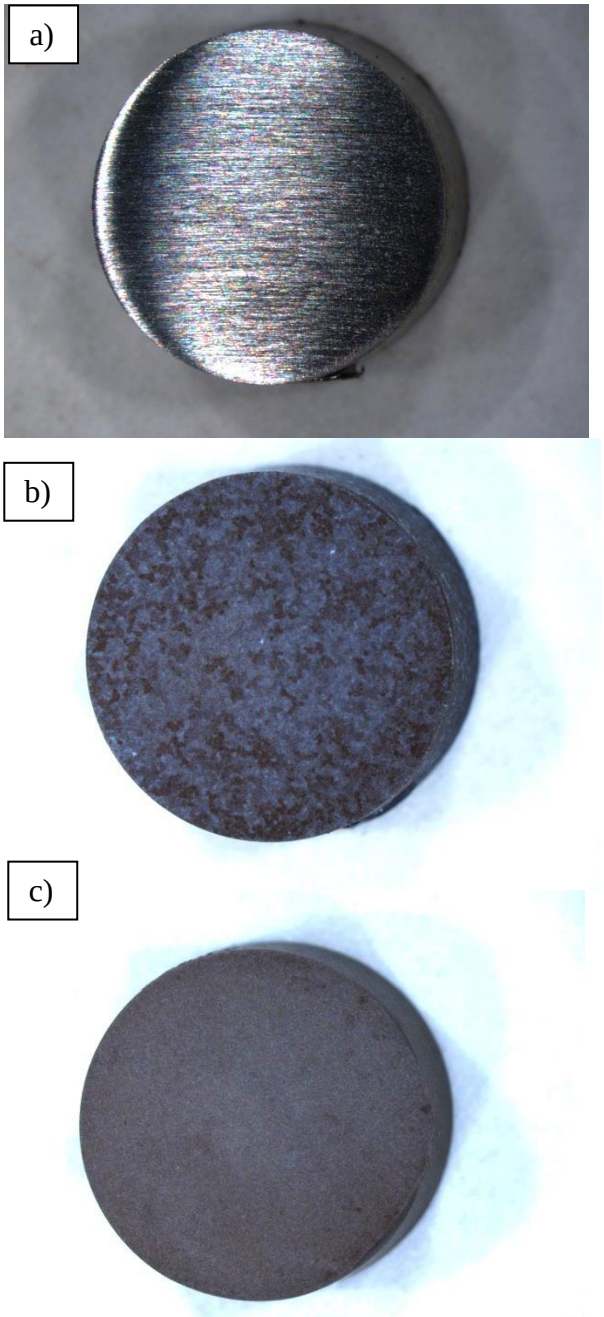

Figure 4.23 : a) Uncoated Ti6Al4V, b)64-MAO, c)64-MAO-Zn.

64-MAO			64-MAO-Zn		
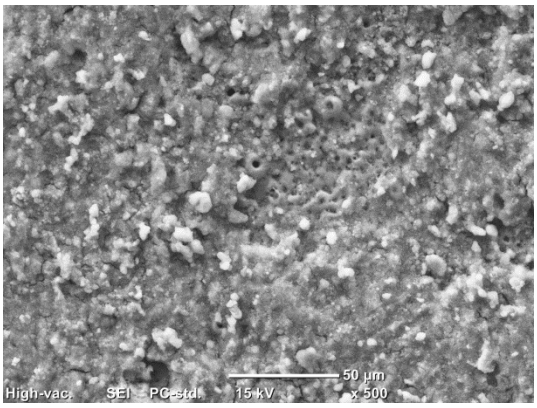			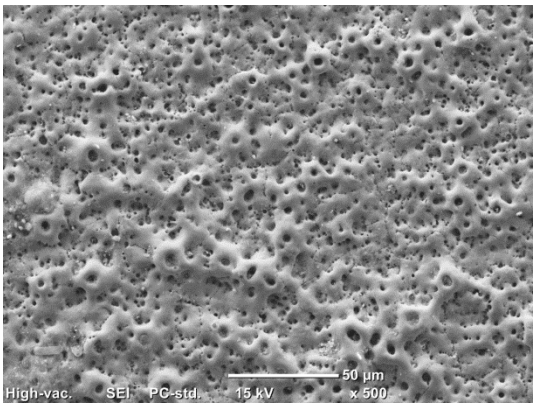		
Element	wt. %	atom%	**Element**	wt. %	atom%
Titanium	1.70	0.78	Titanium	30.35	14.97
Vanadium	0.11	0.05	Vanadium	0.75	0.35
Aluminium	0.14	0.11	Aluminium	1.86	1.62
Oxygen	51.62	71.01	Oxygen	49.89	73.67
Phosphate	15.86	11.27	Phosphate	2.90	2.22
Calcium	30.57	16.78	Calcium	8.88	5.23
-		-	Zinc	5.38	1.94

Figure 4.24 : Morphology and composition of Ti surfaces: SEM micrographs showing a) 64-MAO and b) 64-MAO-Zn surface morphology, EDS results showing composition of the samples

Figure 4.24 shows SEM images and EDS results of the coated Ti6Al4V surfaces. 64-MAO and 64-MAO-Zn exhibit porous surface, the pore size and the distance between neighbor pores were seemed clearly different. 64-MAO exhibited lower porosity than 64-MAO-Zn. Besides, the associated EDS spectra of the 64-MAO and the 64-MAO-Zn showed that the deposition of Ca and P which generated biocompatible compounds. The atomic ratios of Ca and P are considered Ca/P ratio was calculated as 1.49 and 2.35 for the 64-MAO and the 64-MAO-Zn samples.

Differently from the surface of the 64-MAO sample, the surface of the 64-MAO-Zn sample was also enriched by Zn (5.38 wt.%) owing to the incorporation of Zn from the electrolyte.

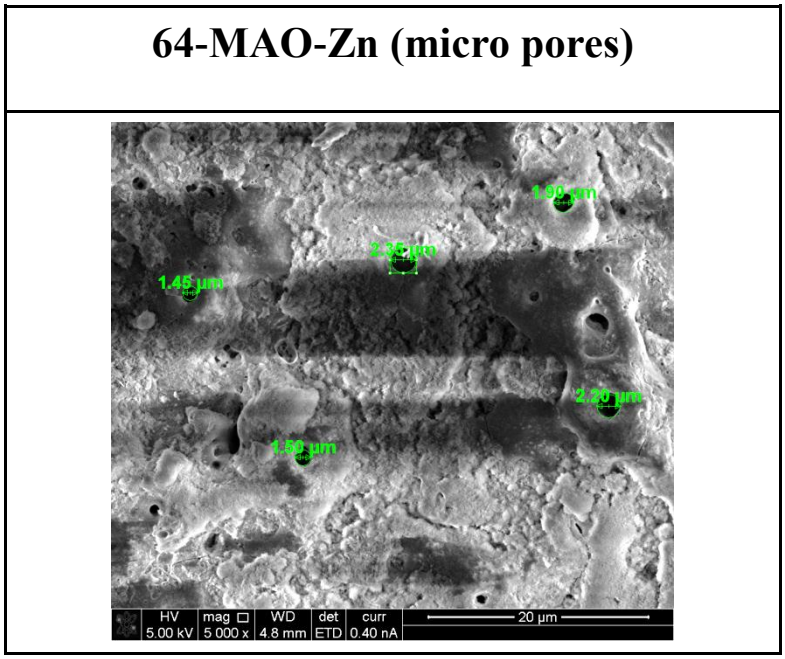

Figure 4.25 : The micro pores of 64-MAO-Zn sample.

On the other hand, the pore sizes of Zn-doped samples showed in Fig. 4.25. Micro pores were observed and the average micro pore size was calculated as ≈ 1.86 µm.

The thickness of the biocompatible compound layers were shown in Fig. 4.26 as below. TiO_2 layers having thicknesses of 754.6 nm for the 64-MAO-Zn sample was observed beneath the biocompatible compound layers. Ca-P containing biocompatible layers of 64-MAO-Zn was ≈ 5.465 µm.

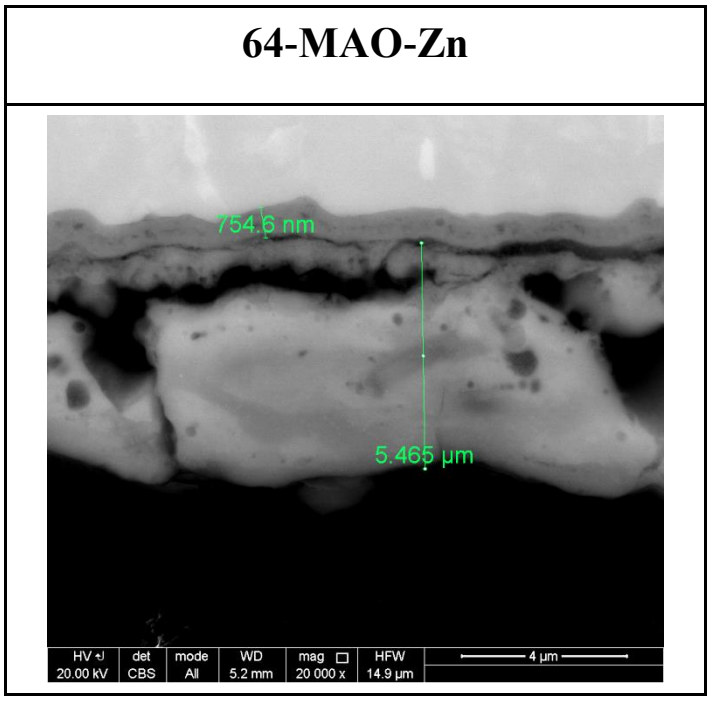

Figure 4.26 : The thickness of MAO coated Zn-doped Ti6Al4V disc.

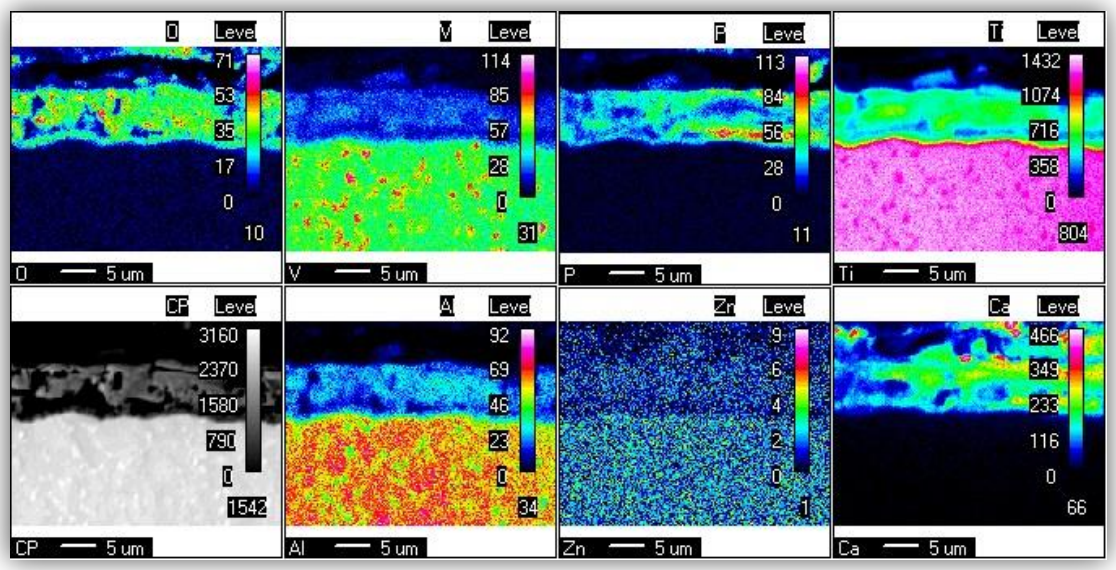

Figure 4.27 : The elemental mapping of 64-MAO-Zn.

EPMA mapping result of 64-MAO-Zn was shown in Fig. 4.27. It can be concluded that Ca, P were distributed over the inner layers of the sample. Ca, P were seemed closed each other. Zn haven't been distributed inner layers.

4.2.3 Surface roughness and wettability

Surface roughness of two different samples (64-MAO, 64-MAO-Zn) were measured, and they are shown in Fig. 4.28. The surface roughness of the 64-MAO appeared to

be higher as compared to that in the 64-MAO-Zn. The Ra values for the 64-MAO and 64-MAO-Zn surfaces were 1.40393µm and 1.26063 µm, respectively.

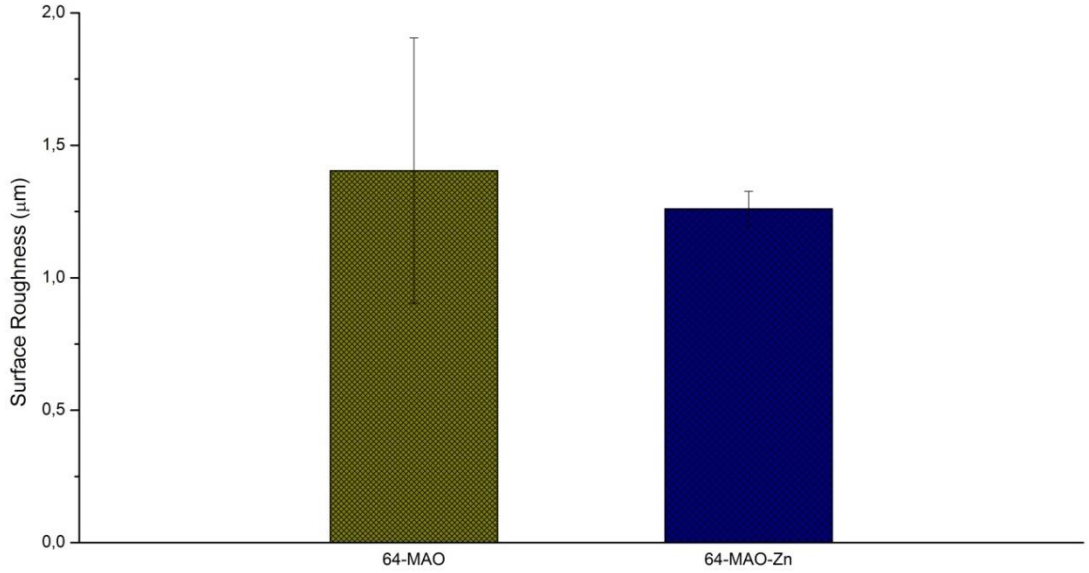

Figure 4.28 : Surface roughnesses of 64-MAO and 64-MAO-Zn.

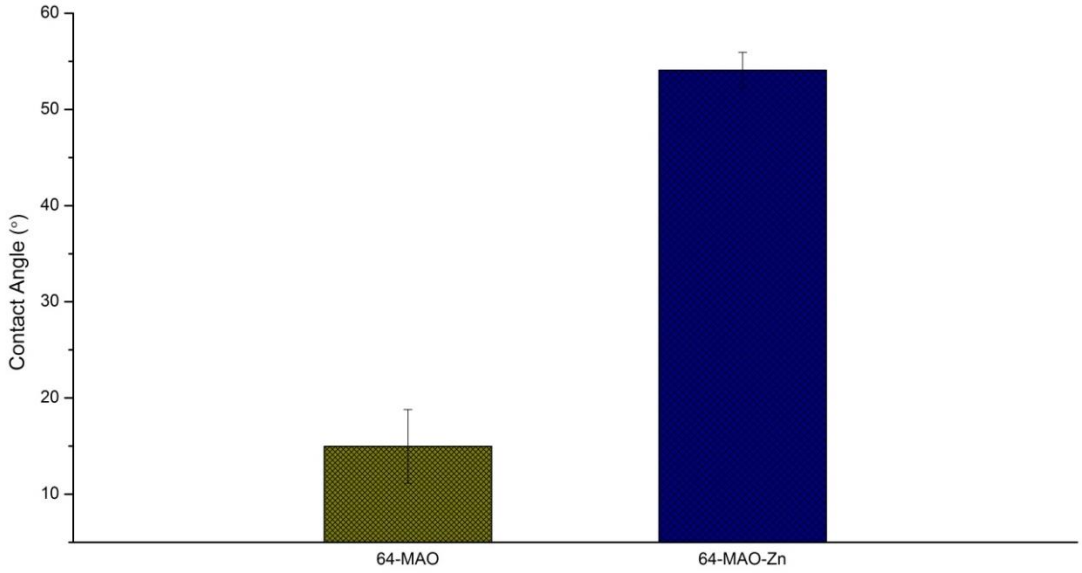

Figure 4.29 : Surface wettabilities of 64-MAO and 64-MAO-Zn.

Surface wettability of two different samples (64-MAO, 64-MAO-Zn) were measured, and they are shown in Fig. 4.29. The surface wettability of the 64-MAO appeared to be lower as compared to that in the 64pTi-MAO-Zn. The contact angle values for the 64-MAO and 64-MAO-Zn surfaces were 14.96857 º and 54.086 º. It

can be observed that Zn-incorporation can increase the hydrophobicity of the surface significantly.

4.2.4 Rockwell C Adhesion Tests

Mechanical properties of 64-MAO, 64-MAO-Zn surfaces were examined by Rockwell C adhesion tests. Rockwell C adhesion tests were conducted on the MAO layers using a Rockwell hardness tester (Zwick ZHR 4150). Rockwell C type diamond cone indenter penetrated into the layers with an applied load of 150 kg. After the Rockwell C adhesion tests, the surrounding area of indent was examined using an optical microscope (OM, Leica ICC50HD).

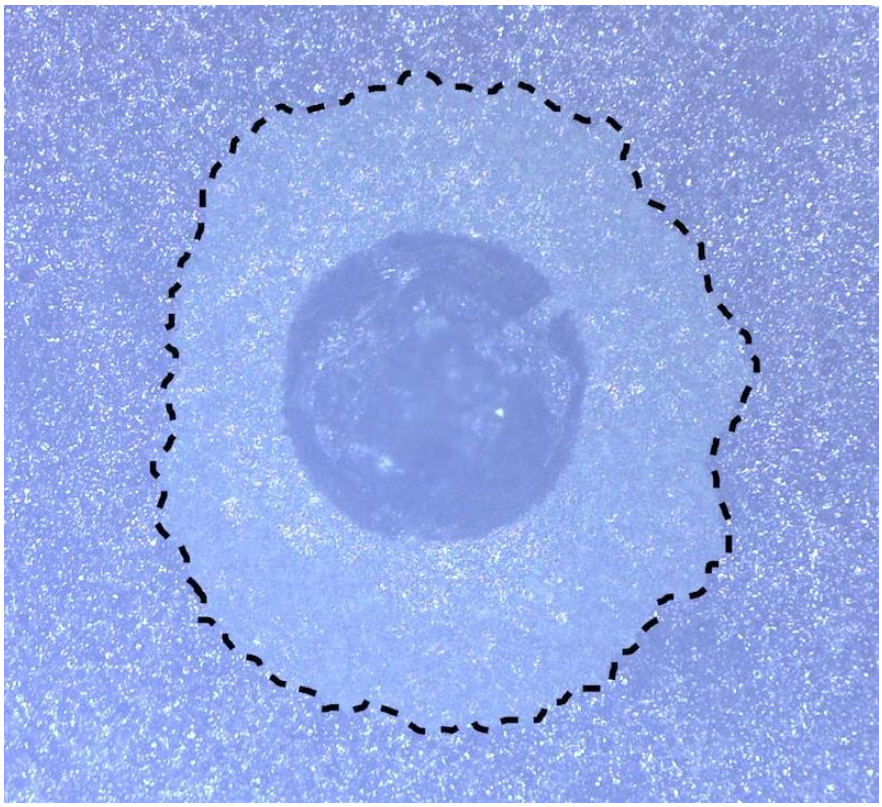

Figure 4.30 : The OM image showing periphery of indent (detached area is encircled) after Rockwell C adhesion test conducted for 64-MAO.

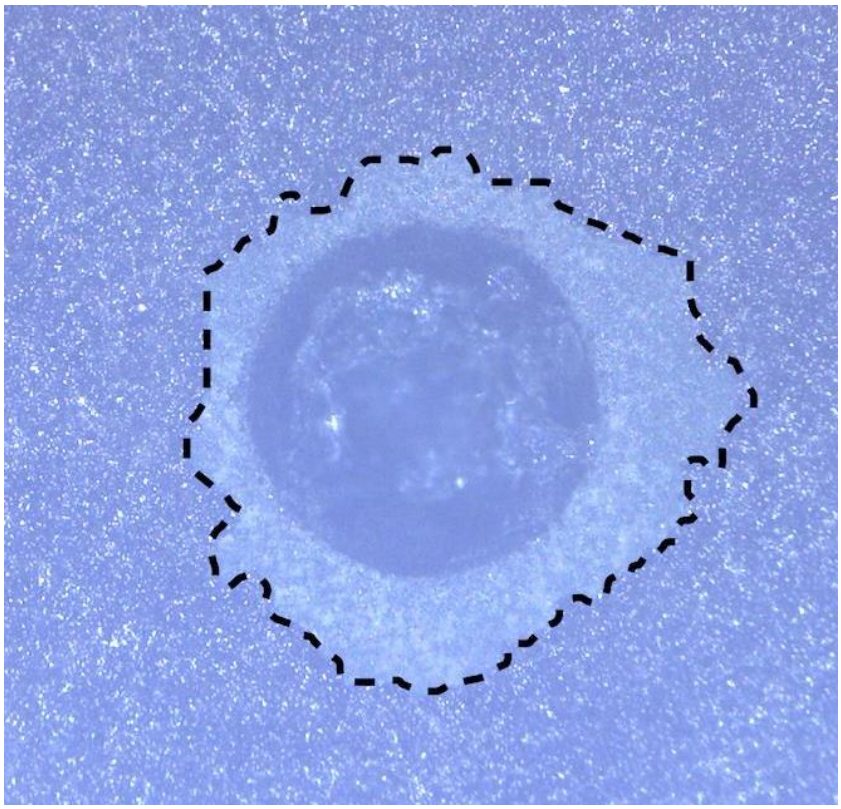

Figure 4.31 : The OM image showing periphery of indent (detached area is encircled) after Rockwell C adhesion test conducted for 64-MAO-Zn.

Results of the Rockwell C adhesion tests are presented as the OM images of the indents and their surroundings at 50X magnification in Fig. 4.30 and 4.31. Delamination zones were detected at the surroundings of the indents. Relatively smaller size of the delamination zone suggests better adhesion for the oxide layer of the 64-MAO-Zn sample as compared with that of the 64-MAO sample.

4.2.5 Ion releasing

Ion releasing from the 64-MAO-Zn was investigated by ICP-OES. The release of Zn ion from the sample into the simulated body fluid (SBF) showed in Fig. 4.32, into the MQ showed in Fig. 4.33.

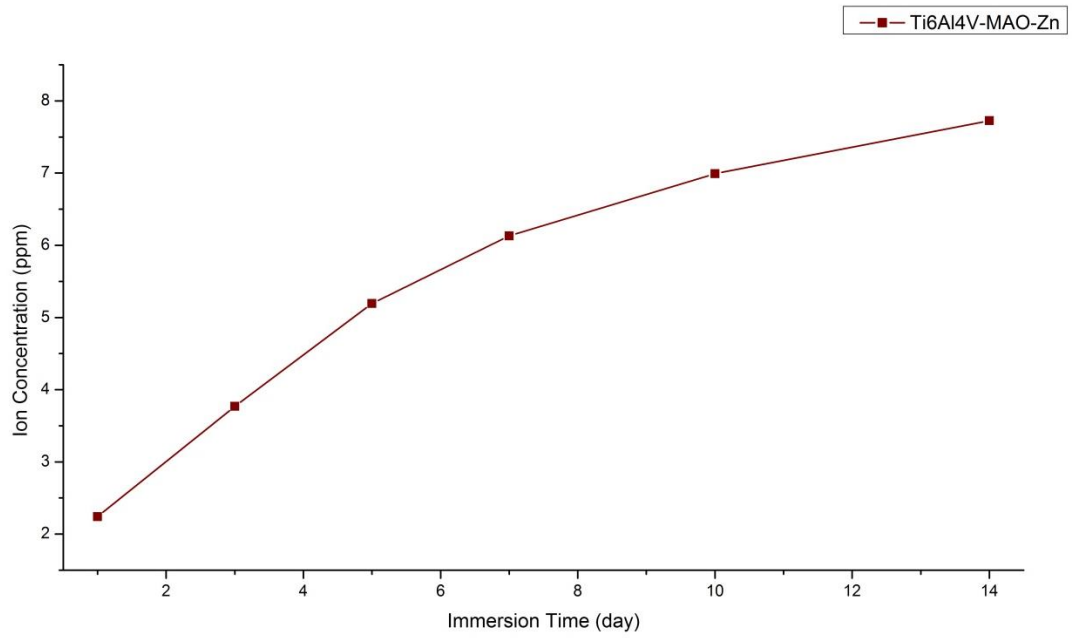

Figure 4.32 : The ion concentration (Zn) into the SBF.

After 14 days, Zn ions were measured and totally 7.727 ppm Zn ions released into the SBF. According to literature, cytotoxicity level of Zn is 10 ppm, so Zn will not be affected as cytotoxic also on Ti6Al4V-based sample.

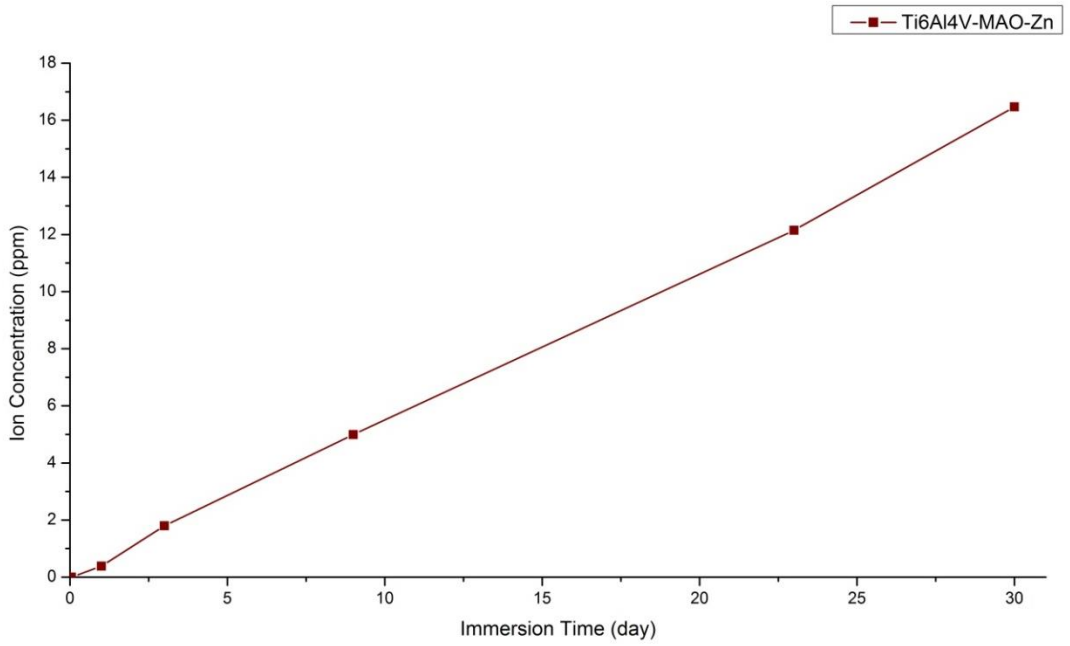

Figure 4.33 : The ion concentration (Zn) into the MQ.

After one month into the ultra pure water, totally Zn ions was measured 16.4715 ppm.

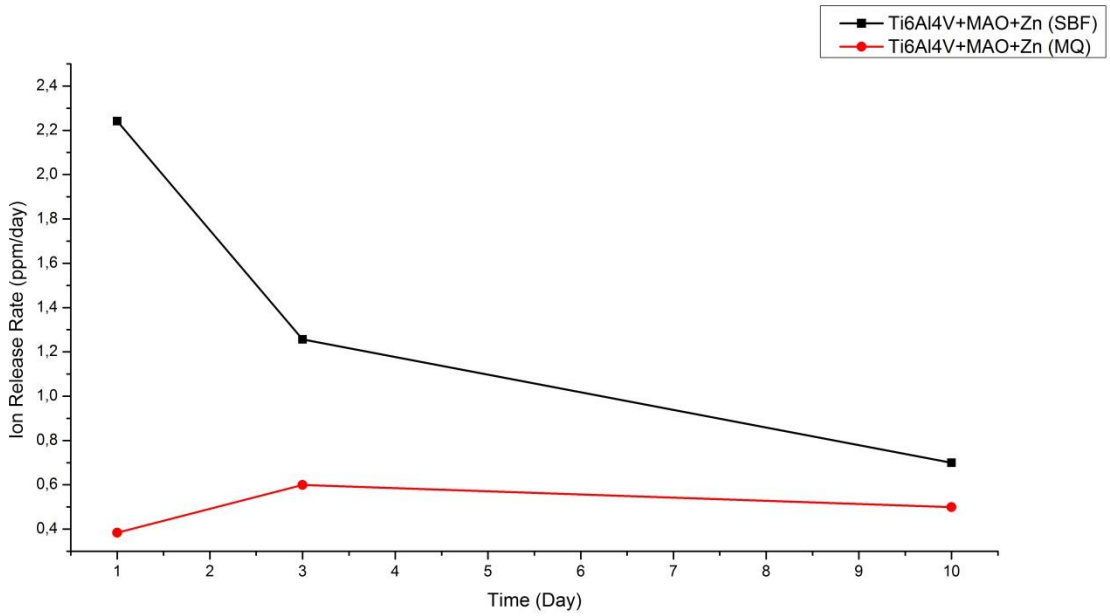

Figure 4.34 : Ion release rate for Ti6Al4V-MAO-Zn into SBF and MQ.

Ti6Al4V-MAO-Zn showed 2.241 ppm/day release rate at the first day. After 10 days, it showed 0.6992 release rate into SBF. In the other hand, Ti6Al4V-MAO-Zn showed 0.384 release rate under equal conditions into MQ. After 10 days, final release rate was measured as 0.4994.

5. CONCLUSION

In this study, the Micro Arc Oxidation (MAO) process was applied to pure titanium (CpTi) and titanium alloy (Ti6Al4V) materials. The following results can be drawn from this research:

- A novel multi-layer coating was successfully deposited on Grade 4 quality Cp-Ti and Ti alloy by conducting MAO in a calcium and phosphorous containing electrolyte at 440 V.
- According to the XRD examination of the CpTi-MAO, the coatings are primarily composed of anatase and rutile TiO_2 phases, α-titanium, hydroxylapatatite, $CaTiO_3$. In addition to all these, XRD examination of the CpTi-MAO-Zn, shows different intensities of major phases. On the other hand, MAO treated Ti6Al4V-based samples revealed the presence MAO treated Ti6Al4V indicated the presence of anatase (TiO_2) as a minor oxide phase, rutile (TiO_2) and titanium as major phases in 64-MAO.
- Introduction of zinc acetate and copper acetate into the electrolyte of the MAO process led to incorporation of 4-5 wt.% Zn or 7 wt.% Cu into the multi-layer coating on the CpTi-based samples were measured by EPMA. 4.82wt.% Zn, 2.43 wt.% Cu was specified by EDS. The Zn-doped Ti6Al4V-based samples has been showed 5.38 wt.% Zn by EDS.
- The Zn and Cu were successfully incorporated in the coatings and distributed over the entire coating. The multi-layer coating was composed of biocompatible compound (HA, $CaTiO_3$) layer with an underlying TiO_2 (anatase and rutile) layer.
- The surface morphology of CpTi-MAO, CpTi-MAO-Zn, 64-MAO, 64-MAO-Zn have micro-roughness which may improve osseointegration mechanisms.
- The surface of the CpTi-MAO, 64-MAO and 64-MAO-Zn can be representatived as hydrophilic surface according to contact angle

measurement. But the average contact angle of the CpTi-MAO-Zn surface was determined as 105.01º which is over the 90º lead to be considered as a hydrophobic surface. Hydrophilicity is affected by the incorporation of the zinc.

- Ion releasing test showed that Zn has low released amount than its cytotoxic level during the 14 days into the SBF. This result proved that Zn-incorporated surface will not show a cytotoxic property.

REFERENCES

[1] **Story B. J., Wagner W. R., Gaisser D. M., Cook S. D., Rust-Dawicki A. M.** (1998). In Vivo Performance of a Modified CSTi Dental Implant Coating, The International Journal of Oral & Maxillofacial Implants, 13, Number 6

[2] **Liua X., Chub P. K., Ding C.** (2004). Surface modification of titanium, titanium alloys, and related materials for biomedical applications, Materials Science and Engineering R, 47, 49–121

[3] **Bauer S., Schmukia P., Mark K., Park J.** (2013). Engineering biocompatible implant surfaces Part I: Materials and surfaces, Materials Science, 58, 261–326

[4] **Pohler O.E.M.** (2000). Unalloyed titanium for implants in bone surgery, Injury, Int. J. Care Injured, 31, 7-13

[5] **Eliasa C. N., Fernandesa D. J., Resendea C. R. S., Roestel J.** (2015). Mechanical properties, surface morphology and stability of a modified commercially pure high strength titanium alloy for dental implants, Dental Materials, 31, 1-13

[6] **Elias C. N., Meirelles L.** (2010). Improving osseointegration of dental implants, Expert Rev. Med. Devices, 7(2), 241–256

[7] **Sula Y.T., Johanssonb C., Byonc E., Albrektssona T.** (2005). The bone response of oxidized bioactive and non-bioactive titanium implants, Biomaterials 26, Pg. 6720–6730

[8] **Santos M. C. L. G., Campos M. I. G., Line S. R. P.** (2002). Early dental implant failure: A review of the literature, Braz J Oral Sci., 1, Number 3

[9] **Cochran DL**. (1999). A comparison of endosseous dental implant surfaces. J Periodontol, 70, 1523–1539.

[10] **Barrere F, Van Blitterswijk CA, de Groot K, Layrolle P.** (2002). Nucleation of biomimetic Ca-P coatings on Ti6Al4V from a SBF × 5 solution: Influence of magnesium. Biomaterials, 23, 2211–2220.

[11] **Sena LA, Andrade MC, Rossi AM, Soares GA.** (2002). Hydroxyapatite deposition by electrophoresis on Ti sheets with different surface finishing. J Biomed Mater Res, 60, 1–7

[12] **Esposito M., Hirsch J. M., Lekholm U., Thomsen P.** (1998). Biological factors contributing to failures of osseointegrated oral implants, Eur J Oral Sci, 106, 527–551

[13] **Tsai M. T., Chang Y.Y., Huang H. L., Hsu J. T., Chen Y. C., Wu A. Y. J.** (2013). Characterization and antibacterial performance of bioactive Ti–Zn–O coatings deposited on titanium implants, Thin Solid Films, 528, 143–150

[14] **T. Amna, M.S. Hassan, N.A.M. Barakat, D.R. Pandeya, S.T. Hong, M.S. Khil, H.Y.** (2012). Kim, Appl. Microbiol. Biotechnol., 93, 743

[15] **P. Petrini, C.R. Arciola, I. Pezzali, S. Bozzini, L. Montanaro, M.C. Tanzi, P. Speziale, L. Visai.** (2006). Int. J. Artif. Organs, 29, 434

[16] **Cimenoglu H., Gunyuz M., Baydogan M., Ugurlu F., Sener C.** (2011). Micro-arc oxidation of Ti6Al4V and Ti6Al7Nb alloys for biomedical applications, 62, 304-311

[17] **Huang, Yong H., Yingjun W., Chengyun N., Kaihui N., Yong H.** (2007). Hydroxyapatite coatings produced on commercially pure titanium by micro-arc oxidation, Biomedical Materials, 2, 196-201

[18] **Hench, L. L., Thompson, I.** (2010). Twenty-first century challenges for biomaterials, J. R. Soc. Interface, 7, 379–391

[19] **Rezaie, H. R. & Bakhtiari, L. & Öchsner, A.** (2015). Biomaterials and Their Application, e-book DOI: 10.1007/978-3-319-17846-2

[20] **Khor, E.** (2001). Chapter 4 – Biocompatibility Issues, Chitin, 55-64

[21] **Park, J. & Lakes, R. S.** (2007). Biomaterials: An Introduction, Springer Science Business Media, LLC, 233 Spring Street, New York, NY 10013, USA

[22] **Url-1** <http://www.zimmer.com>

[23] **Williams, D. F.** (1981). Biocompatibility of Clinical Implant Materials, 1st ed., CRC Press

[24] **De Groot, K., Wolke, J. G. C., Jansen, J. A.** (1998). Proceedings Institute of Mechanical Engineers, 137-147

[25] **Davis, J. R.** (2003). Handbook of Materials for Medical Device, 1st edition, ASM International

[26] **Niinomi, M.** (2010). Metals for Biomedical Devices, Woodhead Publishing Limited and CRC Press

[27] **Seshacharyulu, T., Mederios, S. C., Frazier, W. G., Prasad, Y. V. R. K.** (2000). Hot working of commercial Ti–6Al–4V with an equiaxed α-β microstructure: materials modeling considerations, Materials Science and Engineering A, 284, 184-194

[28] **Patial, S. R., Dahotre, N. B.** (2009). Calcium phosphate coatings for bio-implant applications: Materials, performance factors, and methodologies, Materials Science and Engineering R, 66, 1-70

[29] **Ratner, B. D., Hoffman, A. S.** (1996). Biomaterials Science: An Introduction To Materials in Medicine, Academic Press, San Diego, California 92101-4495, USA

[30] **Agrawal, C. M.** (1998). Journal of Materials, 31-35

[31] **Wang, M.** (2003). Biomaterials, 24, 2133-2151

[32] **Cooke, W. F., Lemons, J. E., Ratner, B.** (1996). Biomaterials Science: Properties of Materials, 11-35

[33] **Park, J. & Lakes, R. S.** (2007). Biomaterials: An Introduction, Springer Science Business Media, LLC, 233 Spring Street, New York, NY 10013, USA

[34] **Nielsen, L. E.** (1983). Polymer Physics: Elastic modulus of syntactic foams, 1567–1568

[35] **Brunette, D. M., Tengvall, P., Textor, M., Thomsen, P.** (2001). Titanium in Medicine, Springer-Verlag, NewYork, USA

[36] **Hiromoto, S.** (2010). Corrosion of metallic biomaterials, 99–121

[37] **Fraker, A. C., Ruff, A. W., Sung, P., Van Orden A. C., Speck, K. M.** (1983). Surface preparation and corrosion behavior of titanium alloys for surgical implants. ASTM Special Technical Publication 796, 206-219

[38] **Lide, D. R.,** (1994) CRC Handbook of Chemistry and Physics

[39] **Parks, G. A.** (1965). The isoelectric point of solid oxides, solid hydroxides and aqueous hydroxocomplex systems. Chern Rev, 177–198

[40] **Vidal, C. V., Mun˜oz, A. I.** (2008). Corrosion Science 50, 1954–1961.

[41] **Singh, R., Dahotre, N. B.** (2007). Journal of Materials Science: Material in Medicine 18, 725-761

[42] **Davis, J. R.** (2003). Hand Book of Materials for Medical Devices, 1st ed., ASM International

[43] **Williams, D. F.,** (1981), Biocompatibility of Clinical Implant Materials, 1st ed., CRC Press

[44] **Detsch, R., Mayr, H., Ziegler, G.** (2008). Acta Biomaterialia: Formation of osteoclast-like cells on HA and TCP ceramics, 139-148

[45] **Url-2** <http:// www.cuneyttas.com/How-to-prepare-SBF-solution.htm>

[46] **Song, W., Zhang, J., Guo, J., Zhang, J., Ding, F., Liying, L., Sun, Z.** (2010). Role of the dissolved zinc ion and reactive oxygen species in cytotoxicity of ZnO nanoparticles, Toxicology Lett., 199, 389-397

CURRICULUM VITAE

Name Surname **:** Merve Kübra SAYGI

Place and Date of Birth **:** Kadıkoy/Istanbul, 25.02.1991

E-Mail **:** **saygime@itu.edu.tr**

EDUCATION **:**

- **B.Sc.** **:** 2013, Yıldız Technical University, Chemical and Metallurgical Faculty, Department of Bioengineering